

LIBRARY
Michigan State
University

This is to certify that the thesis entitled

# ADHESION BETWEEN NEXTEL 312<sup>™</sup> FIBERS AND BLACKGLAS<sup>™</sup> SILICON OXYCARBIDE AND ITS EFFECT ON COMPOSITE PROPERTIES

presented by

John Allen Helmuth

has been accepted towards fulfillment of the requirements for the

Master's degree in Materials Science

Major Professor's Signature

May 26, 2003

MSU is an Affirmative Action/Equal Opportunity Institution

# PLACE IN RETURN BOX to remove this checkout from your record. TO AVOID FINES return on or before date due. MAY BE RECALLED with earlier due date if requested.

DATE DUE	DATE DUE	DATE DUE

6/01 c:/CIRC/DateDue.p65-p.15

# ADHESION BETWEEN NEXTEL 312™ FIBERS AND BLACKGLAS™ SILICON OXYCARBIDE AND ITS EFFECT ON COMPOSITE PROPERTIES

Ву

John Allen Helmuth

#### **A THESIS**

Submitted to
Michigan State University
in partial fulfillment of the requirements
for the degree of

**MASTER OF SCIENCE** 

Department of Chemical Engineering and Materials Science

2003

#### **ABSTRACT**

# ADHESION BETWEEN NEXTEL 312™ FIBERS AND BLACKGLAS™ SILICON OXYCARBIDE AND ITS EFFECT ON COMPOSITE PROPERTIES

Bv

#### John Allen Helmuth

Increasing demand for high strength, light weight composite structures for use in gas turbine engine applications has fueled interest in ceramic matrix composites. CMC's typically exhibit high strength with low ductility and often require expensive manufacturing processes, however, a polymer precursor to a ceramic matrix reinforced with continuous ceramic fibers offers high strength coupled with ductile fracture modes. Fabricated with conventional epoxy composite tooling, a Silicon Oxycarbide reinforced with a Boron Nitride treated aluminoborosilicate fibers is capable of meeting 1300°F service environments found in gas turbine engines. This continuously fiber reinforced CMC lends its improved toughness to controlled fiber pull-out during failure which is created through the Boron Nitride interphase. This work characterizes fiber-matrix adhesion of untreated and BN treated Nextel 312™ fibers through fiber pull-out and indentation testing. Contact angle and wettability measurements also are assessed. Flexure and short beam shear testing of both unidirectional and woven composites were used to verify adhesion observations. Environmental Electron Scanning Microscopy (ESEM) performed in conjunction with composite processing provided insight to matrix cracking and fiber-matrix differential expansion effects. This work served to quantify performance gains associated with the BN treatment of Nextel 312™ composites.

#### **ACKNOWLEDGMENTS**

I would like to express my thanks to Dr. L.T. Drzal for his guidance through my graduate studies along with Mr. M.J. Rich and the staff and students of the Composite Materials and Structures Center. Also, I would like to thank Dr. Richard Schalek for his assistance with this project including numerous informative discussions. Additionally, financial and technical support was provided by the Honeywell Corporation (formally Allied Signal, Inc.), Pratt & Whitney Auto Air, Inc., and Jet Engineering, Inc. Finally, I would like to thank my family for their patience and support throughout this extended project, without whom, this would not have been possible.

## **Table of Contents**

List of Table	<b>S</b>			viii
List of Figur	es			ix
Chapter 1:	INTR	ODUC	ΓΙΟΝ	1
Chapter 2:	BAC	KGROU	IND	4
	2.1	Matrix	x Materials	6
		2.1.1	Glass and Glass-Ceramics	6
		2.1.2	Mullite	8
		2.1.3	Alumina	8
		2.1.4	Zirconia	9
		2.1.5	Silicon Carbide	9
		2.1.6	Silicon Nitride	10
		2.1.7	Carbon	10
	2.2	Fiber	Reinforcements	11
		2.2.1	Glass	11
		2.2.2	Alumina	12
		2.2.3	Graphite\Carbon	13
		2.2.4	Silicon Carbide	14
		2.2.5	Silicon Nitride	15
	2.3	Fabric	cation Methods	16
		2.3.1	Hot Pressing	16
		2.3.2	Hot Isostatic Pressing	18

		2.3.3 Chemical Vapor Infiltration	19
		2.3.4 Direct Metal Oxidation	20
		2.3.5 Sol-Gel Method	22
		2.3.6 Polymer Precursors	22
		2.3.7 Silicon Oxycarbide	23
	2.4	CMC Interphase	26
		2.4.1 Mechanical Contribution (Frictional and Residual Stresses)	27
		2.4.2 Chemical Contribution	27
	2.5	Failure Mode	28
		2.5.1 Fiber-Matrix Debonding	29
		2.5.2 Fiber Deformation and Fracture	29
		2.5.3 Fiber Pullout	30
Chapter 3	EXP	ERIMENTAL	32
	3.1	Blackglas <sup>™</sup> Polymer Precursor Reinforced with BN Treated Nextel 312 <sup>™</sup> Fibers	32
		3.1.1 Blackglas™ Matrix System	33
		3.1.2 Nextel 312™ Fibers	34
		3.1.3 Boron Nitride Treatment	34
	3.2	Characterization of as Received, Desized, and BN Treated Nextel 312™ Fibers	36
		3.2.1 XPS Analysis	37
		3.2.2 Auger Electron Spectroscopy	38
		3.2.3 Stress-Strain Measurements	38
	3.3	Composite Specimen Fabrication	40

		3.3.1	Boron Nitride Fiber Treatment	40
		3.3.2	Composite Prepregging	41
		3.3.3	Polymer Cure	41
		3.3.4	Pyrolysis	42
		3.3.5	Reinfiltration Process	42
	3.4	Adhes	sion Measurements	44
		3.4.1	Interfacial Shear Strength	44
		3.4.2	Fiber Pull-Out	46
		3.4.3	Contact Angle and Wettability	46
	3.5	Comp	osite Performance Analysis	47
		3.5.1	In-Situ ESEM Pyrolysis	47
		3.5.2	Flexure Testing	50
		3.5.3	Short Beam Shear Testing	50
		3.5.4	Iosipescu In-Plane Shear Testing	50
	3.6	Fractu	re Analysis	51
Chapter 4	RESU	JLTS A	ND DISCUSSION	52
	4.1	Chara	cterization of Fiber Samples	52
		4.1.1	XPS Results	52
		4.1.2	Auger Spectroscopy Results	57
		4.1.3	Stress-Strain Measurements	57
	4.2	Comp	osite Specimen Fabrication	58
	4.3	Adhes	sion Measurements	62
		4.3.1	Interfacial Shear Strength	62

		4.3.2	Fiber Pull-Out	66
		4.3.3	Wettability	66
	4.4	Comp	osite Performance Analysis	67
		4.4.1	In-Situ ESEM Pyrolysis	67
		4.4.2	Flexure Strength	76
		4.4.3	Short Beam Shear Strength	77
		4.4.4	Iosipescu In-Plane Shear Strength	79
	4.5	Fractu	are Analysis	81
	4.6	Surfac	ce Chemistry of Fracture Surfaces	90
Chapter 5	CON	CLUSIO	ON	96
REFERENC	CES			97

## List of Tables

Table 2.1	Properties of typical reinforcement and matrix materials.	5
Table 3.1	Nextel 312 <sup>™</sup> properties.	34
Table 4.1	Fiber surface chemistry (atomic%).	53
Table 4.2	Sample weight gain through densification cycles.	61
Table 4.3	Interfacial shear strength.	63
Table 4.4	As-received flexure strength.	76
Table 4.5	BN treated flexure strength.	77
Table 4.6	BN treated short beam shear strength.	78
Table 4.7	As-received short beam shear strength.	78
Table 4.8	As-Received Iosipescu in-plane shear strength.	79
Table 4.9	BN treated Iosipescu in-plane shear strength.	80
Table 4.10	Fracture surface atomic concentrations.	93
Table 4.11	Matrix atomic concentrations.	93

# List of Figures

Figure 2.1	Schematic representation of hot pressing equipment.	17
Figure 2.2	Schematic of hot isostatic pressing equipment.	18
Figure 2.3	Schematic of chemical vapor infiltration method	19
Figure 2.4	Process description for directed metal oxide technique	21
Figure 2.5	Preparation of glasses, glass-ceramics and ceramics by the sol-gel process.	22
Figure 2.6	Processing steps required to prepare the four types of polymer derived ceramics.	23
Figure 2.7	Schematic representation of fiber-matrix interphase in a composite material.	26
Figure 3.1	Schematic of interfacial testing system.	45
Figure 3.2	Pyrolysis process.	49
Figure 4.1	ESEM micrograph of as-received Nextel 312™ fiber surface.	54
Figure 4.2	ESEM micrograph of desized Nextel 312™ fiber surface.	55
Figure 4.3	ESEM micrograph of BN treated Nextel 312™ fiber surface.	56
Figure 4.4	Typical weight gain curve.	61
Figure 4.5	IFSS micrograph of as-received sample.	64
Figure 4.6	IFSS micrograph of BN treated sample	65
Figure 4.7	ESEM in-situ pyrolysis. Top: As received fiber composite at 650X and room temperature. Middle: Desized fiber composite at 650X and room temperature. Bottom: BN treated fiber composite at 1500X and 161°C.	70
Figure 4.8	ESEM in-situ pyrolysis. Top: As received fiber composite at 1000X and 300°C. Middle: Desized fiber composite at 1000X and 301°C. Bottom: BN treated fiber composite at 2500X and 327°C.	71

Figure 4.9	ESEM in-situ pyrolysis. Top: As received fiber composite at 600X and 501°C. Middle: Desized fiber composite at 500X and 500°C. Bottom: BN treated fiber composite at 1500X and 499°C.	72
Figure 4.10	ESEM in-situ pyrolysis. Top: As received fiber composite at 1000X and 599°C. Middle: Desized fiber composite at 1000X and 600°C. Bottom: BN treated fiber composite at 1500X and 600°C.	73
Figure 4.11	ESEM in-situ pyrolysis. Top: As received fiber composite at 600X and 900°C. Middle: Desized fiber composite at 850X and 900°C. Bottom: BN treated fiber composite at 1500X and 900°C.	74
Figure 4.12	ESEM in-situ pyrolysis. Top: As received fiber composite at 3050X and 900°C. Middle: Desized fiber composite at 1500X and 1000°C. Bottom: BN treated fiber composite at 2500X and 901°C.	75
Figure 4.13	BN Treated and As-Received Flexure Load vs. Displacement. Illustrating .05% strain to failure for as received and .5% for the BN treated flexure samples.	77
Figure 4.14	Mechanical testing summary.	80
Figure 4.15a	Delaminated desized composite sample at low magnification.	84
Figure 4.15b	Delaminated desized composite sample at high magnification.	85
Figure 4.16a	As received low magnification fracture surface.	86
Figure 4.16b	As received high magnification fracture surface.	87
Figure 4.17a	BN treated low magnification fracture surface.	88
Figure 4.17b	BN treated high magnification fracture surface.	89
Figure 4.18	Schematic diagram illustrating the possible locus of failure.	92
Figure 4.19	EDX spectra taken from a matrix region exposed during fiber pull-out (4.19a) and an enlargement of the low energy section of (4.19a) shown in (4.19b).	94
Figure 4.20	(4.20a) EDX spectra taken from the fiber surface showing the presence of boron and nitrogen and (4.20b) an enlargement of the low energy section of the spectra shown in (4.20a).	95

## Chapter 1

#### INTRODUCTION

Recent cost reduction goals coupled with aggressive performance requirements have hastened the development of structural composite materials utilized in hostile operating The aerospace and power generation industries demand increased environments. performance from their respective products through the incorporation of high performance structural materials. Components fabricated from advanced materials must be capable of meeting operating temperatures in the 1000°F to 2500°F regime, withstand supersonic air velocities, and resist both thermal oxidative degradation and erosion. Gas turbine engine and ground based power generation applications will benefit from the incorporation of these materials as weight reductions and efficiencies gained from increased combustion temperatures elevate specific power ratings. Component examples include exhaust tailcones, interturbine seals, and thrust vectoring surfaces. Additionally, performance in automotive applications is expected to increase as turbocharger rotors, valves and piston rings are designed with advanced composite materials to reduce weight and enhance wear resistance. Materials capable of operating in these environments have been researched for many years and several candidates are under consideration.

Traditionally utilized high performance alloys have performed adequately in the aforementioned operating environments but suffer from property degradation due to long term elevated temperature exposure and hot gas corrosion. The weight associated with the most commonly used alloys is typically three times that of conventional composite structures,

which are primarily polymer composites. Although advanced polymer matrix composites have served industry well in replacing ferrous and nonferrous metallic structures they typically are limited to exposure below 600°F, which warrants the continued development of high temperature composite materials.

Composite materials capable of operating in the 1000°F to 2500°F have been developed but reinforcement and matrix interactions have not been fully understood. Metal matrix composites (MMC) have exhibited increased elevated temperature properties and offer "tailorable" properties unlike conventional alloys. The MMC has been developed to improve upon the performance of conventional high performance alloys by adding the stiffness and weight reductions offered by platelet, particulate, and fibrous reinforcements. This combination of materials demonstrates specific strength gains over traditional alloys, but MMC are also susceptible to degradation at elevated temperatures. MMC structures demonstrate a thermal expansion mismatch phenomenon resulting in fiber damage as stresses between the matrix material and reinforcement material build during thermal cycling. While numerous fiber and reinforcement treatments have been studied, the inherent coefficient of thermal expansion mismatch phenomenon continues to hamper progress [1].

While many ceramic materials are stable at temperatures of 1000°F to 2500°F, they are prone to uninhibited crack growth and do not possess the damage tolerance and load carrying capability required of structural components. The addition of a reinforcement constituent may modify the ceramic matrix to the extent that damage tolerance is increased, as a result, ceramic matrix composites (CMC) potentially will replace many exotic alloys now functioning from 600°F to 2500°F. The CMC future is largely dependent on the complete understanding of structure-processing-property relationships and fiber-matrix

interactions, specifically, as they pertain to composite toughness.

While many materials may be selected for use in hostile environments based on their mechanical performance, several economic concerns must be addressed prior to the final application. Quite often materials, which are researched, have limited availability or require exotic manufacturing processes. In the development phase, caution must be exercised to insure advanced material candidates are selected from readily available sources within acceptable industry cost structures. The aerospace industry has typically been utilized for "high end" material research and development; however, the end product should be accessible to automotive industries as well.

When cost is estimated, the figure is a result of many considerations. A comprehensive review of costs such as raw material, tooling, fabrication, and by-product disposal as well as final component weight reduction, durability and process ability must be made. Traditional alloys such as titanium and nickel-based superalloys have relatively high raw material costs and require expensive tooling schemes for end component fabrication. High temperature MMC structures also utilize titanium and nickel-based superalloys for the matrix constituent in addition to silicon carbide, tungsten or other fiber reinforcements to obtain maximum performance. Fiber and matrix costs for the aforementioned systems are costly and the required fabrication processes such as hot isostatic pressing can be limited by the complexity of component geometry. Ceramic matrix systems, which offer fabrication methods utilizing existing composite tooling and processing methods in conjunction with low cost commercially available reinforcements, are the goal of more recent initiatives.

## Chapter 2

#### **BACKGROUND**

Typically ceramic materials are thought to possess very low toughness and exhibit susceptibility to sudden and catastrophic failure. Throughout ceramic development efforts to increase toughness have been undertaken through the addition of various reinforcements. Particulates, whiskers, chopped fibers, and more recently, continuous fiber reinforcements have been employed to prevent rapid and uncontrollable crack propagation through structural ceramic components.

The key to the CMC development is the "controlled" propagation of cracks and the subsequent dispersion of crack energy within the laminate structure. A laminate structure, which exhibits excellent toughness, will attain this attribute through graceful fiber debonding and, under ultimate loading conditions, fiber pullout. This "strain" toughness is coupled with reduced strength as the sliding or debonding nature of the system fails to efficiently transfer the load carried by the brittle matrix to the high strength reinforcing fibers. In the event that the debonding effect is eliminated, which may occur during composite processing or during demanding thermoxidative exposure, the load transfer may become so efficient that the continuously reinforced CMC will perform much like a traditional monolithic ceramic. Characterizing and controlling the interphase, which governs the ductile-brittle CMC, will enable applications to expand. Along with interphase engineering, careful selection of complimentary reinforcement and matrix materials must be made to insure satisfactory performance from the final product. A material overview is provided in Table 2.1.

Table 2.1: Properties of typical reinforcement and matrix materials [2].

	Density	Tensile	Youngs'	Thermal	Fiber
	$(g/cm^2)$	Strength	Modulus	Expansion	Diameter
		(MPa)	(GPa)	(10 <sup>-6</sup> /°C)	(µm)
Fibers:					
High Modulus Carbon	1.8	1900	530	radial 8.0	8.0
High Strength Carbon	1.8	2760	275	axial	-
CVD SiC Monofilaments	3.2	3450	415	4.8	140
Nicalon SiC Yarn	2.6	2060	220	3.1	10-15
Boron Monofilament	2.5	2750	400	4.7	100-200
Boron Nitride	1.9	1380	90	7.5	-
Boron Carbide	2.4	2275	90	4.5	-
Alumina	3.9	1400	385	8.5	20
Alumina-Borosilicates:					
Nextel 312™	2.5	1550	152	5.5	11
Nextel 440™	3.1	2000	190	5.5	11
Whiskers:					
SiC	3.2	21000	840	4.8	0.1-0.6
Alumina	3.9	21000	430	8.6	-
Boron Carbide	2.5	14000	480	4.5	-
Graphite	1.7	21000	700	2.0	-
Silicon Nitride	3.2	14000	380	2.8	-
Matrix Glasses					
& Ceramics:					
Borosilicate Glass	2.3	100	60	3.5	-
Silica Glass	2.3	120	70	0.5-8.6	-
Mullite	2.8	185	145	5.3	-
Si <sub>3</sub> N <sub>4</sub>	3.2	410	310	2.8	-
SiC	3.2	310	440	4.8	-
Alumina (Al <sub>2</sub> O <sub>3</sub> )	3.6	250	330	8.5	-
Zirconia (ZrO <sub>2</sub> )	5.7	140	250	7.6	-

#### 2.1 MATRIX MATERIALS:

The design and fabrication of high temperature structures may be customized for a given environment through the use of many constituent materials. The demands placed on advanced materials today cannot be met by utilizing a single material, but rather, require the benefits achieved by combining materials to form composite structures. Current CMC systems are fabricated from many commercially available constituents and recent advancements in matrix and reinforcement materials have made it possible to target high temperature hostile environments. Matrix materials of interest include, but are not limited to, glasses, glass-ceramics, mullite, alumina, zirconia, silicon carbide, and silicon nitride.

#### 2.1.1 Glass and Glass-Ceramics:

Glass and glass-ceramic materials may be produced in large quantities and have been utilized in flat glass applications, containers, tableware, fiberglass, and specialty glasses requiring additional thermal stability. A wide variety of applications result from low cost of manufacture and tailorable properties. The production of traditional materials such as sodalime-silica glass and borosilicate glass requires silica sand (SiO<sub>2</sub>), which has been sized from 40 to 140 mesh and cleaned to remove any refractory heavy metal impurities, to create the glassy structure. Upon heating materials such as crushed limestone and soda ash through the 700°F to 1500°F range, CaO, MgO, and Na<sub>2</sub>O fluxes are generated with an accompanying evolution of gases which serve to mix the melt. Increasing the melt temperature to 1800°F-2200°F while additions of silica sand are made complete the basic melt required to produce traditional glass products. Additionally, the melt may be supplemented with feldspatic sand, which contains alumina (Al<sub>2</sub>O<sub>3</sub>) to reduce the thermal coefficient of expansion, increase

tensile strength, and improve resistance to chemical attack. In the production of fiberglass and borosilicate specialty glasses used in laboratories, additions of borate rich materials such as borax further increase thermal shock resistance while improving strength [3].

The traditional glass formulations have also been used in structural applications when properly reinforced to enhance toughness. Glass matrix structures reinforced with silicon carbide fibers have been fabricated and exhibit fracture toughness increases from 0.7 ksi√in to 27-ksi√in [4]. Carbon fibers have also been used to reinforce glass matrix composites, however, the melt temperature required for the permeation of the fiber preform results in oxidation of the reinforcement. Applications of glass matrix composites are somewhat limited due to the matrix use temperature limit of 1300°F- 1400°F [5].

The further processing of traditional glasses to produce glass-ceramic matrix compositions has been utilized to enhance thermal stability, strength, and toughness. Glass exhibits a structure, which is noncrystalline and has short-range order. During glass processing, great effort is expended to prevent crystallization because it creates a product, which has poor optical properties in addition to reduced mechanical performance. The controlled crystallization through the incorporation of nucleating agents such as TiO<sub>2</sub> followed by heat treatment to produce a fine grained structure results in a glass-ceramic structure. This matrix material is readily formed into complex shapes and contains near zero porosity. The maximum glass-ceramic matrix service temperature depends on the composition; however, the 1450°F to 2200°F range is typical. Commercially available glass-ceramic systems include Li<sub>2</sub>O-Al<sub>2</sub>O<sub>3</sub>-SiO<sub>2</sub> and MgO-Al<sub>2</sub>O<sub>3</sub>-SiO<sub>2</sub>, which possess near zero thermal expansion coefficients with tensile strengths of 150-170 MPA. The glass-ceramic materials offer improved properties to those of their amorphous glass counterparts and also

may be toughened substantially with reinforcements [6].

Fiber reinforced glass-ceramic composites have been fabricated using a melt process, which begins with a powdered glass and preform. The glass-ceramic precursor is melted into the preform and through subsequent heat treatment the fine-grained crystalline structure is formed throughout the matrix. Silicon Carbide fibers have been utilized in this fabrication process and composite structures with volume fractions approaching 45-50% have been produced [7].

#### **2.1.2** Mullite:

Mullite is regarded as a refractory having the composition (3Al<sub>2</sub>O<sub>3</sub>-2SiO<sub>2</sub>), demonstrating exceptional resistance to thermal shock and low CTE of 5.5 x 10<sup>-6</sup>/°C. Mullite is commonly created by the reaction sintering of Al<sub>2</sub>O<sub>3</sub> and SiO<sub>2</sub> powders at temperatures at or above 1600°C (2900°F). During processing, care is taken to obtain the best possible properties by creating a fine-grained structure without amorphous boundary phases. Mullite structures include monolithic and SiC reinforced composites which demonstrate tensile properties of 200 MPA (29 ksi) and 425 MPA (61.5 ksi) respectively. Mullite is also found in high refractory bricks where corrosion resistance is required [8, 9].

#### **2.1.3** Alumina:

Alumina (Al<sub>2</sub>O<sub>3</sub>) may be utilized in a monolithic form or as the matrix constituent in CMC structures when high temperature stability is required. Al<sub>2</sub>O<sub>3</sub> is formed by the heating of alumina hydrates producing 95-99% pure alumina at temperatures of 1200°C (2190°F). Due to strong chemical bonding, the stable  $\approx$ -Al<sub>2</sub>O<sub>3</sub> structure demonstrates the greatest hardness relative to other oxides and exceptional strength. Alumina monoliths possess tensile strengths of 150-200 MPa at temperatures of 1000°C (1830°F). The processing of

alumina monoliths and composites is typically carried by the compaction of powders. Applications of these structures range from piping linings and cyclones where wear resistance and impact strength is valued to electrical substrates where thermal stability and low electrical conductivity are required [10].

#### 2.1.4 Zirconia:

Zirconia (ZrO<sub>2</sub>) is manufactured from Zircon (ZrO<sub>2</sub>-SiO<sub>2</sub>), which is naturally occurring in beach sands found primarily in Australia and South Africa. The Zircon may be chlorinated with carbon to form zirconium and silicon tetrachlorides, which are later separated through a distillation process. The ZrO<sub>2</sub> is distributed in a powder form, which has been modified with Ca, Mg, or Y to create a stabilized structure consisting of precipitates of tetragonal and or monoclinic phases dispersed in a cubic matrix. This partially stabilized zirconia (PSZ) exhibits excellent chemical resistance, high hardness and melting temperatures approaching 2370°C (4300°F). Alumina modified PSZ (Al<sub>2</sub>O<sub>3</sub>-ZrO<sub>2</sub>) systems demonstrate improved wear resistance and have been utilized as cutting tools. Whisker reinforced tetragonal zirconia polycrystalline composites have been fabricated by hot pressing at 1450°C (2640°F), which further enhances toughness [11].

#### 2.1.5 Silicon Carbide:

Silicon Carbide may be produced as a monolithic structure or processed to contain particulate, whisker, or continuous fiber reinforcement. SiC possesses a structure comprised of strong covalent bonding, which results in thermal and chemical stability. Silicon Carbide has been utilized for electrical resistance heating elements, crucible materials and internal furnace components. Gas turbine applications such as turbine vanes, shrouds and bushings have been produced through hot pressing powders.

In terms of matrix applications found in advanced CMC'S, SiC is typically produced through chemical vapor deposition processes. Reactant gases such as CH<sub>3</sub>SiCl<sub>3</sub>-H<sub>2</sub> or SiH<sub>4</sub>-C<sub>x</sub>H<sub>y</sub> are forced through a fibrous preform, which results in SiC deposition on the fiber surface. The resultant SiC matrix material, when reinforced with SiC, Alumino-silicate fibers or other oxide fibers, demonstrates high strengths approaching 400 MPa and fracture toughness of 18-20 ksi√in (>20 Mpa√m). This matrix material possesses a melt temperature of 2200°C (3992°F). Silicon Carbide matrix composites exhibit resistance to erosion, corrosion and wear allowing applications to develop in hostile engine environments [12,13].

#### 2.1.6 Silicon Nitride:

Silicon Nitride exhibits a variety of mechanical, thermal, and electrical properties depending on the processing method utilized and subsequent structure, which is obtained. Producing silicon nitride is achieved from an initial silicon powder, which is nitrided in molecular nitrogen from temperatures between 1150°C (2100°F) to 1400°C (2550°F). RBSN (Si<sub>3</sub>N<sub>4</sub>) is composed of α and β crystallographic forms and exhibits 12-30% porosity. Complex shapes may be formed with little dimensional change and typical flexural strengths of 22-50 ksi are possible [14]. Components may also be fabricated by hot pressing in graphite dies coated with boron nitride. Hot pressed Si<sub>3</sub>N<sub>4</sub> is processed at temperatures of 1650°C to 1850°C (3000°F to 3600°F) and pressures of 2200-4500 psi. Hot pressed components are limited in complexity due to the uni-axial pressure application.

#### **2.1.7 Carbon:**

Carbon may be used as a matrix material and is most commonly reinforced with 3-D carbon fiber preforms to form Carbon/Carbon composite structures. The carbon preform is typically infiltrated with a phenolic resin and cured to form a rigid structure. A

subsequent pyrolysis in an inert atmosphere carborizes the phenolic and the resultant porous carbon matrix requires chemical vapor infiltration (CVD) processes to fully densify the composite structure. Typically, applications include brake disks for aircraft and high performance automotive applications. The carbon matrix and fiber reinforcement is subject to oxidation degradation over extended periods of high temperature exposure but component weight reductions and improved frictional performance have made carbon a viable matrix material for certain applications.

#### 2.2 FIBER REINFORCEMENTS:

In order to increase the toughness of many monolithic glass or ceramic matrix composites, a variety of reinforcements have been researched. Selection of the fibrous constituent has been governed by factors such as comparable thermal expansion coefficients to that of the matrix and thermal oxidative stability. Fibers such as glass, alumina, alumina-borosilicates, carbon/graphite, silicon carbide, and silicon nitride are options for CMC reinforcement.

#### 2.2.1 Glass:

Glass fibers demonstrate chemical and thermal stability much like the bulk glass and glass-ceramic matrix materials, which makes fiberglass reinforcements attractive for aggressive environments. Bulk glass fiber production is most commonly carried out through the direct melt method whereby molten glass is extruded through an orifice creating a fine fiber typically 3 to 20 microns in diameter [15].

Varying the molten glass composition permits the fabrication of three basic forms of commercial glass fiber. E-glass, which possesses a calcium aluminoborosilicate

composition, is a general use grade, which has ambient temperature tensile strengths of 3445 MPa (500 ksi). This fiber is utilized in applications, which demand strength and electrical resistivity. Applications, which require extremely high tensile loading, are best suited for the S-glass magnesium aluminoborosilicate fiber, which exhibit 4585 MPa (665 ksi) ambient tensile strength. C-glass is a soda-lime-borosilicate, which demonstrates 3310 MPa (490 ksi) ambient tensile strength but is highly resistant to chemical attack particularly from acidic compounds [16].

In terms of CMC structures, the glass fibers offer several options to assist in the tailoring of a structure, however, the temperature limitations must be considered. The aforementioned glass fibers have melt temperatures ranging from 1000-1450°C (1825-2650°F) but the mechanical properties are reduced by 50% or more by the 538°C (1000°F) mark, making glass an unacceptable reinforcement for CMC structures operating in the 1000-2000°F range.

#### **2.2.2** Alumina:

Alumina silicate fibers are thought of as glass fibers typically unless the purity exceeds 99%  $\alpha$ -Al<sub>2</sub>O<sub>3</sub> and exhibits a polycrystalline structure. This level of purity and structural order is what defines an alumina fiber, which is utilized most often in metal matrix and ceramic matrix composite structures. The fiber is made by a continuous slurry spinning process of alumina particles in an aqueous solution with organic polymer stabilizers. The fiber is dried at low temperature and then fired to form a dense, high temperature stable  $\alpha$ -Al<sub>2</sub>O<sub>3</sub> fiber. A silica coating is usually applied to the fiber to minimize the effects of surface defects and thus improve the tensile strength, which is 14 to 19 GPa (2 to 2.8-10<sup>6</sup> psi) with a tensile modulus of 390 GPa (57-10<sup>6</sup> psi). The alumina fiber has excellent elevated

temperature stability to 1000°C (1830°F) while maintaining approximately 100% of its tensile strength and modulus [17]. Alumina fibers exhibit the temperature capability for most high temperature applications not requiring service above the 1000°C (1830°F) regime, which makes the fiber a likely candidate for MMC and CMC structures.

#### 2.2.3 Graphite/Carbon:

Carbon fiber reinforcement is used for many high strength lightweight structures. The two fiber forms, carbon and graphite, are often mistakenly interchanged when composite materials are discussed. The hexagonal base structure of carbon is highly structured and exhibits high modulus and tensile strengths. Conversely, the bond strength of the hexagonal planes is relatively weak and thus the transverse load carrying capability of the carbon structure is low. If, during processing, sufficient pretreatment loading and heat treatment is undertaken, a three-dimensional order will be obtained and this high performance fiber is termed graphite. If, however, the fiber is found to have hexagonal planes twisted in relation to each other and some degree of disorder exists the fiber is said to be a carbon fiber. Commercially available material typically utilized in high performance composite structures is the carbon fiber and it is derived from three basic raw materials.

The carbon fiber can be created from Rayon, Polyacrylonitrile (PAN), or Pitch based precursors. In each of the three cases, the base material is pyrolized to create a carbon fiber. Rayon has the poorest conversion rate and produces the lowest modulus end product while the PAN and pitch based fibers can be processed to create very high modulus fibers in excess of 725 GPa (110 x 10<sup>6</sup> psi). The carbon fiber may be heat treated in an inert atmosphere to temperatures of 1000-3000°C (1830-5430°F) to form varying modulus properties with the ultrahigh modulus fibers undergoing the highest thermal processing. At the conclusion of the

basic fiber production, a variety of treatments may be applied to tailor the carbon fiber toward its end use.

The carbon fiber may be treated to improve its handling characteristics, adhesion to various matrix materials and ability to resist thermal oxidation. Fiber tows are often coated with an epoxy resin to prevent fiber damage as the tows or bundles are taken up on a spool or woven into cloth. The fibers are also typically coated or sized with hydroxyl and amine groups to improve laminate performance. Finally, carbon fibers have also been treated with SiC, BN and other thermally stable compounds to protect the base fiber from oxidation. Carbon fibers serve as an excellent composite reinforcement; however, their primary limitation is rapid oxidation rates at temperatures above 700°F (370°C). Research has been conducted to limit the oxidizing effects at elevated temperatures with various coatings, however, due to the thermal mismatch between the coating and the fiber, cracking in the protective barrier along with diffusion effects, the fibers are still susceptible to degradation during extended service conditions. As a result the use of carbon fibers has been limited for the environments targeted for CMC structures [18].

#### 2.2.4 Silicon Carbide:

Silicon Carbide fibers are manufactured by two distinctly different methods, which yield a fiber capable of reinforcing either MMC or CMC structures. The first method produces bicomponent fibers that are formed by first taking a carbon core and subsequently depositing, via chemical vapor deposition, the bulk SiC about the core to create a finished fiber with an average diameter of 10-15  $\mu$ m. The second method produces a monolithic fiber by polymer pyrolysis and is commonly referred to as the Nicalon SiC fiber. Both of the carbide SiC fiber structures demonstrate advantages over other oxide fibers, in that, they

possess superior mechanical properties, especially higher modulus of elasticity and axial compression in the case of large diameter fibers. The mechanical properties of the SiC fiber are desirable for CMC reinforcement; however, the fiber is susceptible to thermal oxidation above 1100°C (2010°F) due to grain microcrystallization. Despite the oxidation at these temperatures, the SiC fibers show promise for CMC reinforcement as additional knowledge is obtained with fiber sizings as they pertain to the oxidative stability [19].

#### 2.2.5 Silicon Nitride:

Silicon Nitride fibers are currently under development but show great promise for CMC reinforcement as bulk matrix Silicon Nitrides, particularly B-Sialon, has shown excellent thermal oxidative stability and mechanical properties. The catalysts utilized for the pyrolysis of polysilazanes has been developed and will be used to create Si<sub>3</sub>N<sub>4</sub> fibers through a spinning process which yield a precursor fiber that may be heat treated much the same as PAN based carbon fibers. The service temperature of these fibers could reach 1500°C (2730°F) with tensile strengths of 1000MPa (145 ksi) and tensile modulus of 300GPa (45-10<sup>6</sup> psi). Ultimately, the final fiber properties will depend on the fiber mechanical pretreatment and thermal processing used during processing, but the Silicon Nitride family of matrix and fiber materials shows promise for superior CMC structural composites [17].

The aforementioned matrix materials and fiber reinforcements are the most widely utilized in the fabrication of high performance composite structures and a summary of their properties has been shown in Table 2.1. The key to a successful material selection for a given fiber\matrix system is the careful evaluation of several criteria including service condition, mechanical and thermal interactions between fiber and matrix along with the final component geometry as it relates to the processing method. Several of the fiber\matrix

combinations may appear to serve well in an application but consideration to part geometry and fabrication method must be undertaken.

#### 2.3 FABRICATION METHODS:

The variety of materials available in the fabrication of high performance composite components is also accompanied by a diverse assortment of processing methods.

#### 2.3.1 Hot Pressing:

Uniaxial hot pressing of ceramics is most probably the oldest technique of forming components but also is the most limited with respect to part complexity which may be achieved. Hot pressing of components requires construction of a mold with corresponding inserts, which define the part shape and size. Pistons and punches, which transmit the externally applied pressure to the die cavity, must be assembled. The appropriate powder, having been previously sized, dried and binder prepared is loaded into the mold. The mold assembly is placed in the furnace\press cavity and pistons are engaged with the pressure source as shown in Figure 2.1. The furnace parameters derived for the particular material to be processed must be programmed into the furnace controller. With the preparation of material, tooling, and press equipment completed, the pressure and heat may be applied to begin the cycle. After the consolidation process has been run to completion, the heat is removed and the component is allowed to cool under pressure before removal from the press. Examples of a typical parts is a flat plate, round billet or a cube with subsequent machining or grinding required to finish the raw shapes into final usable products.

Boron Carbide (BC<sub>4</sub>) is a specific material traditionally hot pressed to form wear

resistant items such as blasting nozzles and wear plates. The  $BC_4$  powder which is <10 $\mu$ m is typically mixed with sintering additives such as Al, Cu, or  $B_2O_3$ . The mixture is pressed at 2100°C (3800°F) for 30 minutes at 35 MPa (5 ksi). [20]

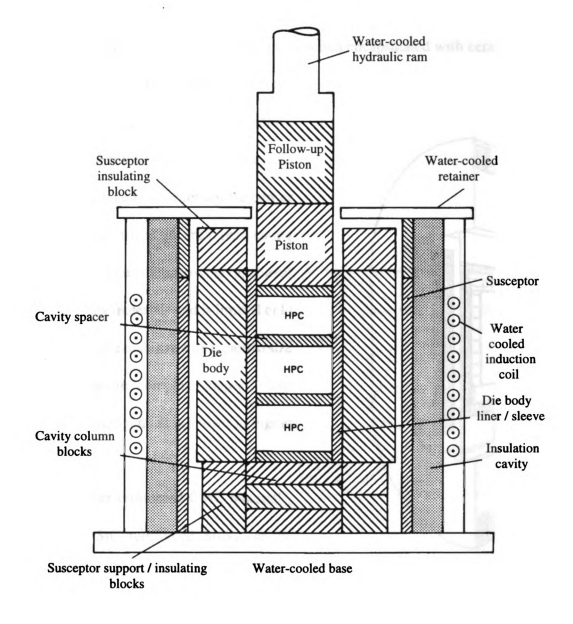


Figure 2.1: Schematic of hot pressing equipment [20].

#### 2.3.2 Hot Isostatic Pressing:

interatomic bond strength along with no part deformation during pressure application. Powders are compacted prior to the HIP process and encapsulated with ceramic, metal or glass barriers. The purpose of the encapsulation is twofold, first, it provides a media in which the pressurizing gas may be uniformly distributed and secondly, the barrier prevents the pressurized gas from permeating the work piece. The HIP process is capable of processing many materials and is limited only by the equipment capability with regard to size and ability handle complex shapes.

Whisker reinforced CMC materials, in particular, SiC reinforced Si<sub>3</sub>N<sub>4</sub> can be processed by the HIP process. Typically, temperatures of 1950°C (3540°F) and pressures of 250 MPa (35 ksi) for several hours are required to fully densify the material.

general press arrangement is shown in Figure

2.2.

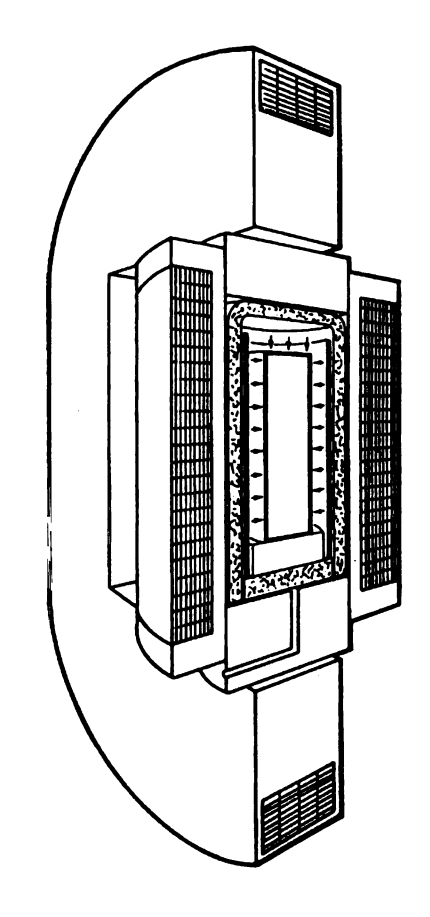


Figure 2.2: Schematic of hot isostatic press equipment [21].

Hot isostatic pressing is an extension of uniaxial hot pressing. The pressure is

applied uniformly and in a direction normal to all part surfaces and results in high

Components fabricated with this process were tested in three point bending and achieved 1000 MPa (150 ksi) flexure results. The HIP process may also be used to produce precision pieces which are dimensionally very accurate as pressed and in the case of textile handling guides fabricated from Si<sub>3</sub>N<sub>4</sub>, demonstrate exceptional wear properties. The HIP process is traditionally utilized to produce smaller components and solid plates, round billets or cubes which are subsequently processed to yield finished parts. The size limitation of typical HIP furnaces creates problems when large structures are encountered but the performance achieved by HIP produced components makes them an important option for the CMC designer [21].

#### 2.3.3 Chemical vapor infiltration (CVI):

Chemical vapor deposition has been used to create various coatings and fibrous reinforcements for wear resistant, electronic, corrosion resistant and oxidation resistant

applications. Carbides, nitrides, oxides and borides have been processed utilizing the vapor deposition method. The process includes heating a substrate fiber, component or panel and depositing a solid via a gas phase to the substrate surface. CVD processes include a furnace to enable the

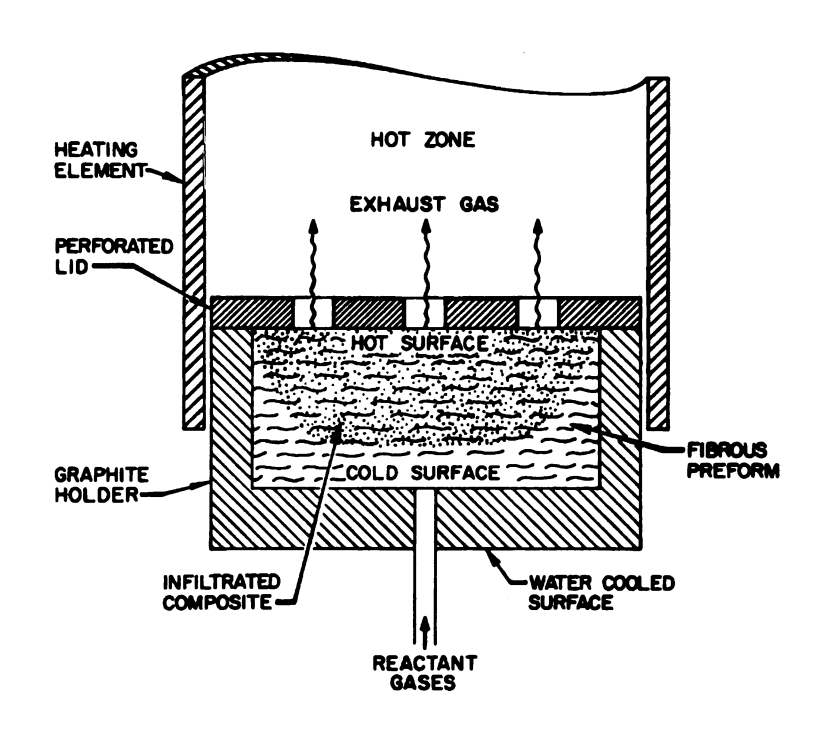


Figure 2.3: Schematic of chemical vapor infiltration method [22].

substrate heating and a means of flowing reactive gases used in the deposition process to and from the substrate. In terms of CMC structures the basic concept of CVD is used but the target becomes a fibrous preform that requires densification with a suitable matrix material. The ensuing densification is termed chemical vapor infiltration and is used to densify CMC structures requiring high temperature performance. Figure 2.3 illustrates this process.

The CVI technique used to densify CMC performs is an isothermal/isobaric process that utilizes low concentration reactant gases to complete densification. The process must be carried out slowly as the preform may become sealed on the surfaces without a reasonable diffusion path remaining to densify the center of the preform. Despite slow process parameters, thick CMC sections will typically require a light surface machining as an intermediate process step to that of the infiltration to open interconnected pores and restore efficient diffusion paths. The process lends itself to large batch production but for larger, high-density components the process time can be several months [22].

#### 2.3.4 Directed Metal Oxidation:

The process of directed metal oxidation has been researched for nearly twenty years with the primary goal of producing composite structures capable of performing in applications such as turbine engine hot sections, piston engine combustion components and other high temperature scenarios that require performance at temperatures up to 2000°C (3630°F). The manufacture process for a high performance CMC begins with an inert barrier placed at the surface of the fiber preform to prevent surface oxidation and the preform assembly including the parent metal alloy are placed in the mold as shown in Figure 2.4. The heating process takes the barrier film, preform, and parent metal to a condition that begins oxidation of the parent metal. As the metal is oxidized, the matrix is created thus densifying

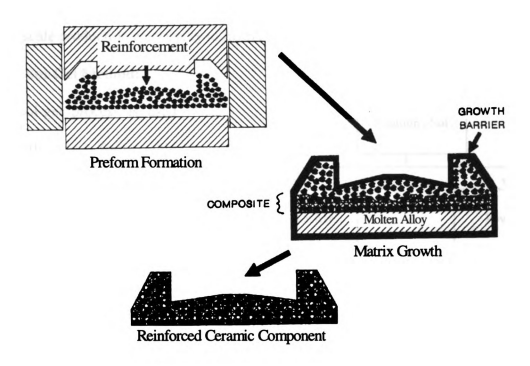


Figure 2.4: Process description for directed metal oxidation process [24].

the CMC. The properties of the CMC are tailorable, in that, the preform architecture may be engineered to meet specific requirements and the matrix properties may be modified as a function of the heating process.

An example of the directed metal oxidation process is SiC reinforced Al<sub>2</sub>O<sub>3</sub>, which has been completed to form heat exchangers, and related furnace components. The aluminum parent metal is placed between the SiC preform layers and the matrix is grown to complete the CMC. The matrix oxidation process has been shown to penetrate preform fiber bundles to create a dense CMC when using untreated Nicalon SiC fibers and pretreated fibers. The composites demonstrate 460 MPa (67 ksi) four-point flexure results at room temperature with a 25% reduction in strength at 1400°C (2550°F). Fracture strength is 27.8 MPa√m (25.3 ksi√in.). The performance of these composites has led to the widespread manufacture of components but the tooling cost to mold at elevated temperatures has made

large-scale production a necessity to justify molds and related processing equipment. [24]

Powder

powders

Uniform

compact

ceramic

#### 2.3.5 Sol-Gel Method:

The sol-gel process is used Solution / Sol primarily form thin to coatings, films, fibers and Powder-free microballoons. Sol-gel techniques use hydrolyzable alkoxides, which undergo a Preform Monodispersed chemical synthesis to form high purity glass, glass-Crystalline **Amorphous** ceramic, and ceramic structures. The material may Glass be amorphous or crystalline which is determined with the Glass-ceramic Polycrystalline Polycrystalline ceramic initial solution or sols and the subsequent processing Figure 2.5: Preparation of glasses, conditions used [23]. Sol-gel sol-gel process [23]. process is shown in Figure

glass-ceramics, and ceramics by the

2.5.

#### **2.3.6 Polymer Precursors:**

Polymer precursors have been used as means to capture the best of the low temperature-processing world combined with high temperature ceramic component production. The process involves the use of a preceramic polymer such as polysilastyrene, vinylic polysilane, polysilazanes or silicon oxycarbides. Much like carbon\carbon composite fabrication, these preceramic polymers are prepregged onto a unidirectional or woven

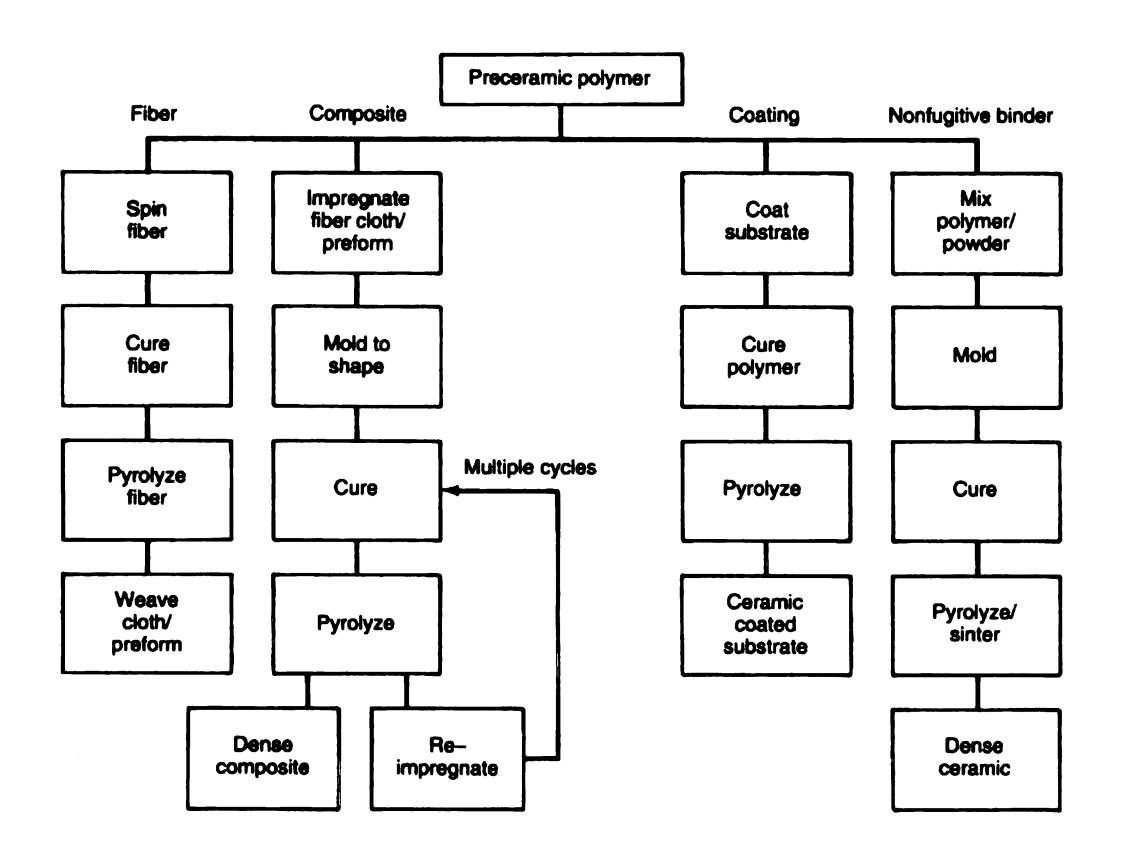


Figure 2.6: Processing steps required to prepare the four types of polymer derived ceramics [25].

ceramic fiber materials and subsequently handled as standard epoxy prepreg materials. After the initial cure and subsequent pyrolzation, the polymer transforms to an amorphous ceramic material. Refer to Figure 2.6 for process flow diagram [25].

#### 2.3.7 Silicon Oxycarbide:

The cure cycle for silicon oxycarbide precursor matrix material is typically low enough to utilize tooling found in the manufacture of fiber reinforced epoxy composite components. The preform or prepreg material is placed on the mold surface with fiber orientation taken into consideration, vacuum bagged and cured under pressure in an autoclave. Typical silicon oxycarbide polymer processing temperatures are 150°C (304°F) and pressures range from 35-100 psi depending on part geometry and tool configuration.

After autoclave cure, the part is removed from the mold and placed in a furnace or kiln.

The pyrolysis process is completed with the component free standing during the initial pyrolysis cycle or basic support surfaces may be provided via alumina blocks. The pyrolysis is carried out in an inert atmosphere typically consisting of free flowing nitrogen. A typical cycle utilizes a ramp rate of 2°F/minute from room temperature to 1700°F and a soak at 1700°F for 1 hour. After the soak period, the ceramic structure is slow cooled to room temperature where it is reinfiltrated to increase its density and reduce open porosity.

During the polymer-ceramic conversion the matrix material undergoes a substantial density change from 1.25g/cm<sup>3</sup> to 2.5g/cm<sup>3</sup>. This increase in density is accompanied with matrix shrinkage and an increase in open porosity thus necessitating the polymer precursor reinfiltration process. The reinfiltration process consists of numerous composite infusions with low viscosity preceramic polymer material to fill porosity. The infiltrations are usually performed with the part under vacuum to aid in the polymer infusion throughout the part thickness. The polymer is cured and the composite is again pyrolyzed to convert the newly introduced polymer to a ceramic. Typically, five or six infiltrations will be utilized to achieve open porosity levels of 3-5% and a final density of 2.25-gm/cm<sup>3</sup> [26].

The polymer precursor materials offer a unique advantage over many other CMC matrix systems with respect to the fabrication methods required to produce finished goods. Previously described CMC processing methods including hot pressing, chemical vapor deposition and directed metal oxidation require the design, development and fabrication of

tooling capable of dimensional stability during processing temperatures ranging from 900°C (1652°F) to 1950°C (3540°F). The thermosetting polymer precursor technology offers initial cure temperatures of 304°F (150°C) to cross-link the polymer. This temperature regime allows traditional epoxy tooling to be used for complex CMC processing during the initial fabrication step. The subsequent pyrolyzation process is typically completed "free-standing" in a furnace that eliminates the need for costly tooling capable of CMC elevated temperature processes. The flexibility to use existing polymer composite and aluminum tooling in the fabrication of prototype and demonstration components has increased the speed at which insitu monitoring of finished components can be achieved. The demonstration components, which include exhaust tailcones, thrust vectoring surfaces and exhaust gas mixers, have provided valuable material design feedback with respect to oxidation, sonic fatigue, and mechanical property degradation.

The aforementioned CMC materials typically suffer from the effects of long-term oxidation resistance at elevated temperatures. The matrix, which has been reinforced with a whisker or continuous fiber, may lose its strain to failure and damage tolerance capability as oxidation degrades the reinforcements ability to toughen the structure. Controlling the fiber-matrix interphase in an effort to prevent subsequent interactions while maintaining a viable load path to arrest crack propagation is the most significant CMC issue currently. The interphase stability issue will be addressed in this research through the survey of various fibers pretreatment to provide an interphase capable of meeting the demands of current high temperature applications.

#### 2.4 CMC INTERPHASE

The interphase existing between fiber and matrix is best considered a threedimensional transition region. This interphase region, as shown in Figure 2.7, depicts a diffuse area between the fiber and matrix, which effects overall composite properties [27]. The interaction of individual fiber and matrix bulk properties, fiber topography, morphology and chemistry, along with fiber sizing will determine the composite performance. The degree of adhesion between fiber and matrix as well as failure mode may be understood from examining this three dimensional region.

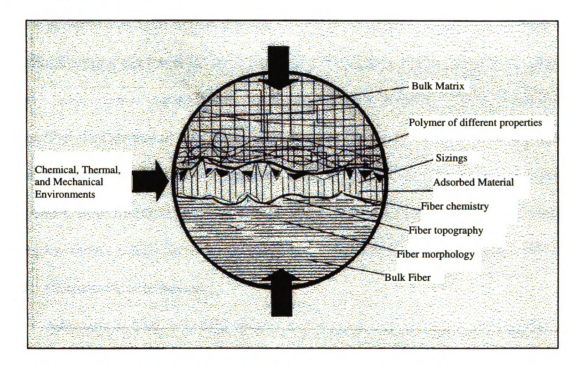


Figure 2.7: Schematic representation of fiber-matrix interphase in a composite material [27].

Adhesion between reinforcement and matrix materials is comprised of several interrelated factors including mechanical, chemical and constituent bulk property interactions. The degree of fiber-matrix adhesion found in a composite structure will determine its strain capability. Understanding the contribution of each factor toward the total

bond strength will serve to better predict overall composite performance and allow an estimation of failure modes-mechanisms [2].

## 2.4.1 Mechanical Contribution: (Frictional & Residual Stresses)

The mechanical contribution toward overall fiber-matrix performance is comprised primarily on fiber topography and residual stresses resulting from differential expansion coefficients between constituents. The surface roughness of reinforcing fibers will result in an increase of fiber pull-out force required to overcome frictional effects. Matrix materials, which have a larger thermal expansion coefficient than that of the reinforcing fibers, will yield a compressive force imparted to the fiber surface, which in turn will increase the effective fiber pull-out force. At the conclusion of CMC processing, it is quite possible to achieve large residual radial stresses between the fiber and matrix. These stresses may induce fiber damage and or matrix cracking which may serve to undermine the interphase region rendering it incapable of carrying crack energies efficiently through a given component. Both frictional and CTE effects can be quantified via single fiber indentation testing and the resulting load data may be used to obtain interfacial shear stresses [28-30].

#### **2.4.2 Chemical Contribution:**

Adhesion in CMC's is also influenced by the chemical bond between fiber and matrix. Strong interaction between fiber and matrix as a result of thermal oxidation is a common problem as the interdiffusion of matrix and fiber materials can create a near monolithic ceramic structure. This degree of bonding will adversely affect the composite properties. If the interface bond is too strong, matrix cracks propagate normal to the fibers, cutting through the fibers without deflection. This fracture behavior causes the composite to have low fracture toughness as indicated by the flat fracture surface. To obtain the desired

fibrous, flaw-tolerant, failure requires a sufficiently low interfacial bond strength such that a propagating crack causes fiber- matrix interfacial debonding and/or deflection of the matrix cracks. Toughness and strength performance can be understood from studying fiber sizings and surface modification effects [2,29].

#### 2.5 FAILURE MODE:

CMC failure modes are of great interest to design engineers as these materials are implemented in areas requiring structural load carrying capability. The failure must be graceful and predicable unlike most monolithic ceramics. As composites are dynamically loaded in service, energy due to impact may occur. This sudden energy input must be uniformly distributed throughout the structure to avoid catastrophic failure. When crack energy travels through the matrix, it will encounter the fiber reinforcement at which time a controlled debonding between fiber and matrix is desirable. The controlled debonding will serve to dissipate crack energy along the fiber axis throughout the structure. In the case of a balanced isotropic lay-up, the energy will be distributed uniformly and thus minimize local catastrophic failure.

The incorporation of treated fiber reinforcements targets the control of CMC failure modes and enhances composite toughness. Toughness or strain capability is generally less than 0.1% for monolithic structures while toughened systems may achieve rates in excess of 0.5% [31]. Failure mode research should consider the effects of chemical bonding, frictional /push-out forces and matrix cracking relationships to describe overall CMC failure characteristics.

### 2.5.1 Fiber-Matrix Debonding:

The chemical bond between fiber and matrix must be sufficient to facilitate load transfer but weak enough to yield slipping between the two constituents. In composites consisting of a mullite matrix and Nextel 440<sup>TM</sup> fiber, hot pressing at temperatures of 1410°C (2570°F) resulted in a fiber-matrix reaction which fused the two constituents together resulting in a brittle fracture. The same Nextel 440<sup>TM</sup> fiber, when BN coated, did not react with the matrix and allowed cracks to propagate along the fiber length indicating that the BN treatment sufficiently prevented chemical bonding [2,29,32,33].

The work associated with fiber debonding from the surrounding matrix can be quantified by considering the interfacial shear stress ( $\tau$ ), the fiber diameter (d), the debonded length ( $l_d$ ) and the difference in strain ( $\Delta \varepsilon$ ) [34-38].

Per fiber basis:

$$W_{df} = F \cdot d$$

$$W_{df} = (\tau \bullet A) (\Delta \epsilon \bullet l_d)$$

$$W_{df} = \tau \pi dl^2 \frac{\Delta \varepsilon}{2}$$

#### **2.5.2** Fiber Deformation and Fracture:

Matrix cracking is best controlled and distributed when a controlled debonding occurs. The work of deformation and fiber fracture can be expressed as the product of the fiber tensile strength ( $\sigma$ ), diameter and debonded length divided by the fiber tensile modulus ( $E_f$ ). The critical transfer length is substituted for the debonded length in the instance that a complete unbond does not exist [34-38].

Per fiber basis

$$W_{\rm ff} = (\frac{1}{2})\sigma_{\rm f}^2 \Delta \epsilon l$$

$$W_{\rm ff} = (\frac{1}{8}) \frac{\sigma_f^2 \pi}{E_f} d^2 l_d$$

$$W_{\rm ff} = \frac{\sigma^2 \pi d^2 l_d}{8E_f}$$

#### 2.5.3 Fiber Pull-Out

Fiber surfaces, which are sufficiently smooth, will contribute to low frictional effects and consequently promote the fiber pull out needed to prevent catastrophic failure. The work associated with pulling a fiber from the matrix is the product of the shear stress and the pull-out length [34-38].

Per fiber basis

$$W_{pf} = (\tau A)l_p$$

$$W_{pf} = \tau n dl_p^2$$

The total work associated with the crack energy can be summarized as follows:

$$W_{t} = \tau n d l_{d}^{2} \frac{\Delta \varepsilon}{2} + \frac{\sigma_{f}^{3} n d^{3} l_{d}}{32 \tau E_{f}} + \tau n d l_{p}^{2}$$

The summation includes the contribution from fiber debonding, deformation-fracture and pull-out. The common component found in the total work relationship is the interfacial shear stress, which is non-linear and contributes to maximum energy adsorption at a specific optimal point.

With the importance of interfacial shear strength on composite toughness highlighted, a closer review of the fiber pretreatment and matrix interactions is necessary. Materials

development and processing of ceramic matrix composites that fail in a high strain (>0.5%), damage tolerant manner are continually being sought. This active research area has lead to the development of silicon oxycarbide/Al₂O₃ composites [39,40,43] and for the production of complex-shaped components at low cost. Aluminoborosilicate/silicon oxycarbide composites have demonstrated the ability to retain enhanced fracture toughness and strength [41,42]. The objective of this work is to extend this research area by correlating the macromechanical properties with the fiber- matrix micromechanical properties of Nextel 312™ fiber/Blackglas™ composites. In particular, an understanding of how the boron nitride coating affects the fiber/matrix adhesion, mechanical properties, and composite failure behavior will be investigated.

## Chapter 3

#### **EXPERIMENTAL**

The experimental work performed in this research program was concentrated toward Nextel 312™ fibrous reinforcement composited in the Allied Signal 493 Blackglas™ preceramic polymer matrix system. This preceramic CMC system offers ease of processing and elevated service temperature benefits but as in many CMC systems requires fiber pretreatment to enhance overall mechanical properties. The goal of this effort is to quantify the stress-strain benefit gained from the use of nitrided Nextel 312™ fibers in the Blackglas™ matrix as compared to either organically treated or bare Nextel 312™ fiber reinforcements. Experimental efforts were divided into two sections consisting of constituent characterization and finished composite property evaluation. Additionally, the Blackglas™-Nextel 312™ composites were monitored *in-situ* during the polymeric conversion to the ceramic in order to gain processing insight with respect to fiber matrix interactions.

# 3.1 BLACKGLAS™ POLYMER PRECURSOR REINFORCED WITH BN TREATED NEXTEL 312™ FIBERS:

While a variety of CMC systems are commercially available, the polymer precursor systems offer the greatest processing flexibility and low initial process temperatures and pressures. The Blackglas<sup>™</sup> polymer precursor system produced by Allied Signal and reinforced with 3M Nextel 312<sup>™</sup> woven fabrics shows promise in the ongoing research for a

toughened, continuously reinforced CMC. The Nextel 312<sup>™</sup> fabric has been enhanced by the addition of a BN rich surface treatment, which creates a stable interphase, capable of facilitating load transfer and crack deflection at the matrix-fiber interface. The BN rich region also provides a barrier to prevent fiber-matrix reactions that may reduce toughness as elevated processing or service temperatures are encountered. The Allied Signal and 3M CMC materials are commercially available and are able to be processed via commercially available equipment.

## 3.1.1 Blackglas™ Matrix System:

The matrix system developed by Allied Signal Inc. is a polymer precursor to a ceramic. The Blackglas<sup>™</sup> 493 polymer is a thermoset produced by the addition reaction of proprietary siloxane monomers and the density of the cured polymer is 1.09 g/cm<sup>3</sup>. The proprietary polymer precursor is cured and subsequent pyrolysis in an inert atmosphere at 900°C (1652°F) causes the conversion to the amorphous silicon oxycarbide SiC<sub>x</sub>O<sub>y</sub> with evolution of Methane and Hydrogen as the byproducts of the phase conversion. This highly refractory, silicon based glass contains 15-30% atomically distributed carbon, has a typical composition of 24 wt% Carbon, 47 wt% Silicon, 28 wt% Oxygen, < 0.4 wt% Hydrogen, < 0.1 wt% Nitrogen (Si C<sub>1,21</sub>O<sub>1,06</sub>) and has been patented as Blackglas™ by Allied Signal Inc. The matrix, while in the pyrolysis cycle, demonstrates a char yield from the polymer state of approximately 81 to 86 % by weight. The pyrolysis results in an amorphous silicon oxycarbide glass retaining 43 to 45% of its initial volume and exhibiting open porosity ranging from 20-30%. Upon the completion of the reinfiltration process, a fully densified matrix is optimized at approximately 0.08 lbs./in<sup>3</sup> (2.2 g/cm<sup>3</sup>). The matrix material is easily reinforced with ceramic fibers to form CMC structures [44].

## 3.1.2 **Nextel 312™ Fiber:**

The 3M corporation

Table 3.1: Nextel 312<sup>™</sup> properties.

produces the Nextel 312™ ceramic				
fibers. The alumina-silica ceramic				
fiber has a composition of 62%				
Al <sub>2</sub> O <sub>3</sub> , 24% SiO <sub>2</sub> , 14% B <sub>2</sub> O <sub>3</sub> .				
Nextel 312™ fibers are available in				
a wide variety of forms including				
fabrics, tapes, sleevings and				
cordage. Due to the variety of forms				
available, Nextel 312™ may be used				
in any number of design				
environments. Typical physical				
properties are summarized in the				
Table 2.1. The fiber surface may be				
modified via CVD or diffusion				
methods to promote a suitable				
interface for a number of ceramic				

Physical Properties	
Composition	62% Al <sub>2</sub> O <sub>3</sub> , 24% SiO <sub>2</sub> , 14% B <sub>2</sub> O <sub>3</sub>
Color	White
Length	Continuous
Fiber Density	2.7 gm/cc
Fiber Diameter (elliptical)	Minor axis: 7-9 micron
	Major axis: 10-12 micron
Surface Area	<1m <sup>2</sup> /gm
Mechanical Properties	
Tensile Strength	1725 MPa (250,000 psi)
Tensile Modulus	138 GPa (20 x 10 <sup>6</sup> psi)
Elongation	1.20%
Thermal Properties	
Continuous use Temperature	1204°C (2200°F)
Short Use Temperature	1371°C (2500°F)
Lineal Shrinkage 2000°F (1093°C)	1.25%
Melting Point	1800°C (3272°F)
Thermal Expansion Coefficient (25-500°C)	3.0 x 10 <sup>-6</sup> DL/L/°C)
Specific Heat	0.25 BTU/lb/°F or Cal/gm/°C
Electrical Properties	
Dielectric Properties	5.2 @ 9.375 x 10 <sup>9</sup> hertz
Optical Properties	
Refractive Index	1.57

matrices. The Nextel 312<sup>™</sup> reinforcement may be preimpregnated as any typical epoxy prepreg material [45,46]. Table 3.1 summarizes various mechanical and physical properties of Nextel 312<sup>™</sup>.

## 3.1.3 Boron Nitride Treatment:

The fiber pretreatment utilized to tailor the debonding process with Nextel 312™

reinforcements is described within a patent created at the Boeing Company. The process involves heating the Nextel 312<sup>™</sup> fabric in an atmosphere containing ammonia, hydrogen and nitrogen at a temperature of 2200-2600°F (1204-1427°C) for a period ranging from 5-90 minutes [47,48]. This process diffuses boron from the fiber bulk structure to the fiber surface, reacts it with ammonia, and produces a thin, uniform boron nitride layer. The coating transitions gradually from the BN surface to the parent boria (B<sub>2</sub>O<sub>3</sub>) found in the bulk fiber thus creating a very stable interface for CMC fabrication [49].

While there are other methods of establishing the BN surface prior to compositing, these methods usually involve exposing the fiber to a liquid boron oxide or boric acid, which severely degrades the oxide based Nextel 312<sup>TM</sup> fiber. Alternatively, the BN surface may be created via CVD or sol-gel methods but maintaining a uniform coating thickness is difficult especially in woven fabrics. In the CVD process, the reactant gasses create the BN coating on the first hot surfaces they come in contact with and maintaining accessibility to all fiber surfaces at constant temperature and with uniform gas composition is difficult. Likewise, the sol-gel method is limited in the solution deposition uniformity. In any case, these methods create a distinct coating unlike the previously described nitriding method developed by the Boeing Company [50-56].

The nitriding method previously described under several patents was further investigated with respect to process sensitivity for time, temperature and reactant gas concentration. SIMS data indicates the NH<sub>3</sub> reactant gas concentration, which was varied from 5% to 20% had no effect on the coating depth or resultant BN concentration. The nitriding process appears to be more sensitive to the time duration that was varied from 15, 30, 60, and 120 minutes. Under these process times and at 1150°C (2102°F), the maximum

weight percent of boron present ranged from 10-22% at 25-50 angstroms. The boron concentration tapered off in all cases to 5-8% at a depth of 100 angstroms from the fiber surface. The 60-minute duration caused the highest concentration of boron at 23-wt% located 35 Angstroms from the fiber surface. Using the 60-minute duration, the experiment was run again varying process temperatures. Temperatures of 1150, 1225 and 1250°C (2102°F, 2237°F, 2282°F) were used to understand their impact to BN formation. All peak concentrations were within 21-23-wt% under this process profile but the higher temperatures yielded a more broad depth profile with boron detected down to 5-8 wt% at 150 angstroms. In summary, the 60-minute time at 1250°C (2282°F) yielded a 22-wt% boron concentration at a depth of 70 angstroms. Appreciable (<8wt%) quantities of boron were noted at depths of 120 to 130 angstroms [57].

# 3.2 CHARACTERIZATION OF AS RECEIVED, DESIZED AND BN TREATED NEXTEL 312™ FIBERS:

Nextel 312<sup>TM</sup> fibers, as received from 3M, are treated with an organic sizing to protect the fiber and facilitate handling through the spooling process. The fiber was examined in this "as received" condition but also examined after a cleaning or stripping process was conducted to expose the base fiber surface and finally an assessment was conducted with a BN treatment present.

The as received fiber has a slight light gray appearance and is somewhat stiff as it is removed from the spool. The fiber tows were used for the base fiber surface characterization and the tows had approximately 3-5K filaments each. The desizing or cleaning process is achieved by heating the sample Nextel 312<sup>TM</sup> in a ventilated furnace to 550°C (932°F) for 12

hours. After heat cleaning, the fibers appear bright white and will be more flexible and soft to the touch. After the fiber desizing, one half of the desized fibers were BN treated via a nitriding process previously described.

The three fiber tow samples were then analyzed to determine the surface composition via x-ray photoelectron spectroscopy and auger spectroscopy. Additionally, the fibers were mechanically assessed to determine if any stress-strain propertied were altered due to the fiber tow processing.

## 3.2.1 XPS Analysis:

The fiber sample surface chemistry was assessed with x-ray photoelectron spectroscopy (XPS). XPS is also referred to as Electron Spectroscopy for Chemical Analysis (ESCA) but the technique will be referred to as XPS throughout this work. XPS analysis begins with the sample bombardment with x-rays in a vacuum of 10<sup>-6</sup> to 10<sup>-10</sup> torr. The impingent x-rays (hv) ionize the sample surface and the emergent core electron energy is detected. The energy input less the core electron binding energy is the detected electron energy as measured by the instrument detector. The relationship is shown below from a physical and energetics viewpoint [58,59].

$$A + hv \rightarrow A^{+e} + e^{-}$$
 (discreet energy-ESCA)

Where A = Atom or Molecule and  $A^{+e} = excited$  ion

$$E \text{ (kinetic)} = E \text{ (photon)} - E \text{ (binding)}$$

Specifically in this work, the Perkin-Elmer model 5400 spectrometer was equipped using a standard Mg Kα<sub>1,2</sub> X-ray (1253.6ev) source operated at 300 watts, 15 kV and 20 mA. The instrument used a 180° hemispherical energy analyzer operated in the fixed analyzer transmission mode at a pass energy of 89.45 eV for survey spectra and 35.75 eV for

multiplex spectra, and a position sensitive detector. Spectra were collected using an analysis area defined by a 3 x 10mm rectangle. Samples were mounted by clamping each end of a two-centimeter length of fiber onto a sample holder using brass clips. All sample handling was done with clean forceps and scissors. Spectra were collected using a 45° degree take-off angle between the sample and the analyzer lens. As received, desized and BN treated fiber tows were examined to determine the surface composition and obtain knowledge regarding the chemistry present.

## 3.2.2 Auger Electron Spectroscopy:

Auger electron spectroscopy (AES) was used to determine the fiber surface composition uniformity and coating thickness if present. The AES technique is similar to the XPS\ESCA technique in that the sample surface is ionized however it is achieved via an electron beam rather than an x-ray source. The impingent electron beam causes vacancies in an inner electron shell as an electron is removed. The vacancies are then filled by electrons from outer shells, which cause x-ray photon emission or the emission of an Auger electron [58,59]. The associated Auger electron energy is detected and used to determine the surface composition within a very specific area. The AES instrument is capable of a spatial resolution of approximately 200Å. The electron beam lateral x-y resolution is approximately .5 μ making it useful for analyzing specific features. The three samples were examined as prepared as well as with a gold coat sputter due to the insulative nature of Nextel 312<sup>TM</sup> fibers. The gold coat was selectively deposited over the fiber surface to prevent sample charging and subsequent sample deterioration while permitting fiber analysis.

#### 3.2.3 Stress-Strain Measurements:

Nextel 312™ fiber mechanical properties were assessed to determine what, if any,

effect the desizing and BN treatment processes may have had on the stress-strain capability. Fibers may be degraded mechanically from the elevated temperature processing required to remove organic sizings and elevated temperatures combined with an ammonia nitriding atmosphere used to create the BN rich surface region. Mechanical tests were performed to assess if any such degradation occurred with particular focus being placed on the BN treated fibers, as the processing parameters are severe.

Single fiber tensile properties for; as received fibers, desized and BN treated fibers have been prepared for tensile evaluation. The single fibers were mounted to stiff rectangular paper frames until the sample could be loaded into the tensile testing machine. Once loaded, the sample was pretensioned and the paper frame was severed allowing the fiber to carry the uniaxial tensile load independently. The United Testing Systems tensile machine was equipped with a micro load cell capable of resolving loads during tensile failure. The samples are to be tested with a crosshead speed of 0.05 inches per minute. This evaluation will determine the residual fiber strength due to processing when compared to the as manufactured condition.

Polymer encapsulated fiber sample fabrication and tensile testing was planned to enable an understanding of the critical fiber fracture length as it relates to interfacial shear strength. The typical carbon fiber-polymer matrix approach includes bridging a single fiber across a dog bone shaped mold and subsequently embedding the fiber in epoxy resin. The sample would then be tested in tension under plane-polarized light to determine the fiber critical fracture length, which is the length where insufficient load can be transferred to the fiber and no further breaks occur. The critical length can be related to interfacial shear strength via the following equation:

$$\tau = \frac{\sigma_f}{2} (\frac{d}{l_c})$$

where (d) equals the fiber diameter, and  $l_c$  is the critical fiber length [60].

## 3.3 COMPOSITE SAMPLE PREPARATION:

Unidirectional samples and woven fabric samples were prepared to accomplish the mechanical property and in-situ pyrolysis evaluations. The sample preparation involves fiber pretreatment, preimpregnation, polymer cure, pyrolysis and finally densification. Composite samples were prepared with as received, desized and BN treated fibers.

#### 3.3.1 Boron Nitride Treatment:

Fibers of Nextel 312<sup>TM</sup> (3M Corp.) aluminoborosilicate (64% Al<sub>2</sub>O<sub>3</sub>, 24% SiO<sub>2</sub>, 14%, B<sub>2</sub>O<sub>3</sub>), with a tensile strength of 1725 MPa and a tensile modulus of 138 GPa, in a 5-harness satin weave fabric woven with 900 denier tows were acquired. The fiber diameter was approximately 12 μm with a coefficient of thermal expansion of 3.0x10<sup>-6</sup>/°C. To protect the fibers from damage and to decrease the amount of interfiber friction, the manufacturer coats each fiber with an organic sizing. In this study, fibers coated with an organic sizing are referred to as "as-received". The as-received fibers were thermally treated to form 2 different fiber surfaces. In the first fiber surface treatment, the fiber was heated from room temperature to 315°C, held for 1 hour and slow cooled to remove the organic sizing. These fibers are referred to as "desized" fibers. The second fiber-surface preparation technique consisted of heating the as-received fibers in a high-temperature ammonia atmosphere. This treatment formed a boron nitride rich surface layer ~200 nm thick and has been reported previously [40]. These fibers are referred to as BN-treated fibers.

## 3.3.2 Composite Prepregging:

The pretreated fibers, either in tow form or 5-harness woven cloth, were prepregged with a Blackglas<sup>TM</sup> preceramic silsesquioxane polymer 493 (Allied Signal, density of ~1.09 g/cm<sub>3</sub>). The fiber tow was prepregged on a Research Tool filament winder. Unidirectional prepreg tape was allowed to have carrier solvents flash-off for improved tact and drape characteristics. Resin to fiber ratio is typically 45% and 55% respectively. Each ply of the tape material was aligned in a 0° orientation to form a true unidirectional composite laminate. The samples were typically (20) plies thick with an average composite panel thickness of 0.100 inches. 2-D woven composite panels consisted of sixteen layers of fabric, which were placed to create a 0/90-balanced lay-up. The solvent flash time and associated resin to fiber content is similar to that of the unidirectional tape. The 5-harness woven fabric panels averaged approximately 0.150 inches thick.

## **3.3.3 Polymer Cure:**

The initial polymer curing of sample panels was performed in a laboratory press without vacuum bagging. The laminate was placed between nonperforated Teflon<sup>®</sup> film to aid in resin containment. Flat shim stock was utilized to create stops, which prevent over bleeding of the laminate and facilitate consistent panel thickness. Panels were consolidated at 30-40 psi while undergoing the cure cycle. The cure cycle ramps from room temperature to 140°F (60°C) at 4°F/minute followed by a hold at 140°F (60°C) for 1 hour. After the initial hold the sample is ramped from 140°F (60°C) to 304°F (150°C) and held at 304°F (150°C) for 1 hour. Following the final hold temperature, the panel is allowed to cool under pressure to room temperature. All samples were deflashed and subsequently cut via a diamond saw into specific coupons for tensile, flexure, short beam shear, Josipescu shear and general-purpose

coupons. Individual samples were then weighed to determine their initial condition prior to pyrolysis.

## 3.3.4 Pyrolysis:

Cured polymer samples were then pyrolyzed to form the ceramic matrix, which is performed in flowing nitrogen to prevent oxidation. The kiln is purged with nitrogen and also slightly over pressured to maintain an oxygen free environment. The samples are placed free standing on flat alumina blocks without additional fixturing. The heating is from room temperature to  $1652^{0}$ F at  $2.25^{0}$ F\min. After this ramp phase, the samples are allowed to stabilize at  $1652^{0}$ F for 1 hour and are finally slow cooled to room temperature at which time the Nitrogen gas flow is halted.

#### 3.3.5 Reinfiltration Process:

Upon removal from the kiln, the samples require reinfiltration with polymer resin to fill open porosity, which has resulted from the polymer to ceramic phase conversion. The reinfiltration resin utilized is a lower viscosity version of the Blackglas<sup>™</sup> 493 system. Samples have a rough and grit like surface finish, which is lightly abraded to remove debris and aid in opening pores, which the resin may then fill. The sample is then weighed and placed in a vacuum bag containing reinfiltration resin. A vacuum is drawn on the bag containing the samples thus drawing the resin into each sample uniformly. The resin is held within the samples via this vacuum application while the press again consolidates the composites under 30-40 psi. The preform temperature is raised from room temperature to 60°C at a rate of 2.2°C/min and held for 1 hour. After 1 hour, the temperature is raised to 150°C at 2.2°C/min and held for 1 hour. Following this heating segment, the preform was press-cooled to room temperature under an applied load of 30-40 psi.

Following the impregnation step, the preforms were pyrolyzed in flowing nitrogen by heating the preform from room temperature to 900°C at 1.25°C/min and holding for 1 hour. The preform was then slowly cooled to room temperature. Further densification of the silicon oxycarbide ceramic matrix composite occurred by applying 5 reimpregnation cycles. Each reinfiltration cycle was achieved by infiltration and curing of the catalyst-added solution using the procedure above followed by a 1 hour, 900°C pyrolysis. To assess the progress of the densification, one panel was removed after each densification step and reserved for characterization. The status of impregnation is designated by the symbol BG(n) where n ranges from 0 to 5. For example, BG(0) represents a composite with no reimpregnation whereas BG(5) corresponds to the sample obtained after 5 reimpregnations. The fiber volume fraction, measured optically, was 55 to 60%.

Following the densification process, the open porosity was verified using alcohol and calculated using Archimedes principle. The open porosity volume fraction has been previously correlated to baseline sample volumes via Helium pycnometry. (41) Open porosity fraction relative to true sample volume have also been correlated to mechanical test results as a function of the number of infiltrations. From this data, open porosity measurements along with the infiltration number provide a reasonable prediction of mechanical properties. Typically samples processed through five infiltrations as further cycling yields only marginal improvements in mechanical properties while adding significantly to processing cost and time.

## 3.4 ADHESION MEASUREMENTS:

## 3.4.1 Interfacial Testing Systems:

Fiber/matrix interfacial shear strength (ISS) measurements were made using a microindentation test. Refer to Figure 3.1 for schematic of equipment [62,63]. Samples were prepared by mounting composite cross-sections in standard metallurgical mounts. The samples were polished with SiC paper to a grit size of 2000 then wet polished with 0.5 µm alumina powder until smooth. The individual fiber indentations were made using a 5 µm radius diamond indenter and recording the load versus displacement values. The ISS is calculated through the use of a finite-element analysis of the stressed area for each fiber under examination. At least 5 fibers were measured for each type of composite [28,60].

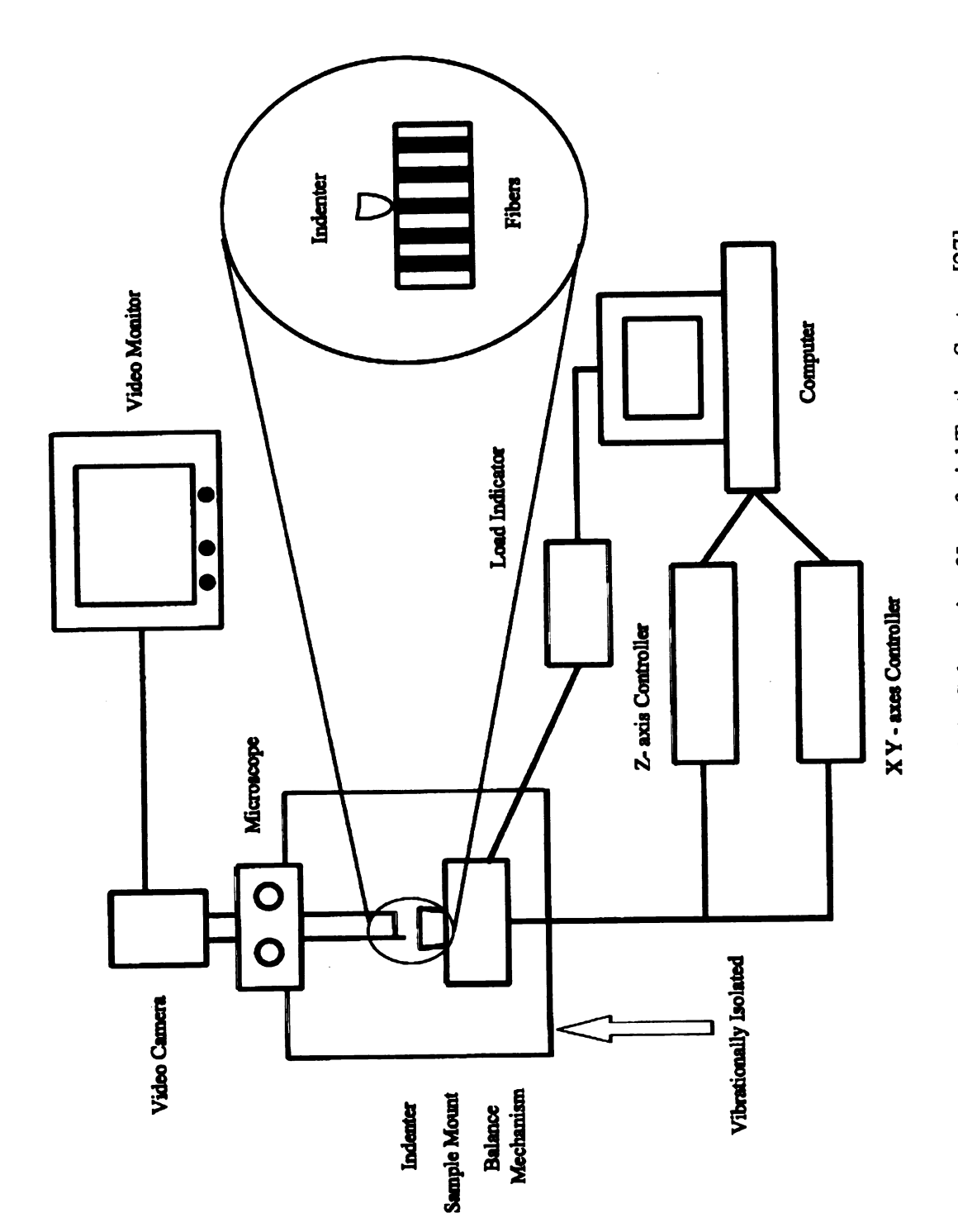


Figure 3.1: Schematic of Interfacial Testing System [27].

#### 3.4.2 Fiber Pull-Out Test:

Sample preparation and testing of Nextel 312<sup>TM</sup> fibers embedded in Allied Signal Blackglas<sup>TM</sup> matrix micro-droplets is a useful means to determine the shear stresses along the fiber-matrix interface as well as determine the frictional nature of the adhesion as the fiber slides through the droplet. The micro-droplet method utilizes a single drop of matrix material applied to the fiber. After the curing and pyrolzation process the droplet is secured in a microvise designed to hold the droplet in a fixed location while allowing the fiber to be drawn from it [45]. The basic relationship is as follows:

$$\tau = \frac{\sigma_f}{2} (\frac{d}{l_c})$$

where  $l_c$  is the embedded fiber length, d is the fiber diameter and  $\sigma_f$  is the uniaxial tensile load imparted on the fiber. This evaluation ignores the varying shear stress distribution along the fiber length which are considered more closely for polymer matrix composites but due to the stiffness associated with the ceramic matrix the above relationship will serve as the beginning benchmark. Once the fiber bond is debonded, the net compressive force on the fiber due to residual curing shrinkage and CTE mismatch will be realized through the following relationship:

$$\tau = \mu \rho_o$$

where  $\mu$  is the coefficient of friction and  $\rho$  is the compressive forces acting normally on the fiber surface [45].

## 3.4.3 Contact Angle and Wettability Measurements

Contact angle and wettability measurements provide insight with respect to the natural affinity for the matrix material to adhere to the fiber. Typically the contact or

surface energy is described as follows:

$$\gamma_{SV} = \gamma_{SL} + \gamma_{LV} \cos \theta$$

where  $\gamma_{SV}$  and  $\gamma_{SL}$  and  $\gamma_{LV}$  are surface free energies of the solid-vapor, solid-liquid and liquid-vapor interfaces respectively as conceptualized from a water droplet on a flat surface. In the case of a fiber surface wetted by an uncured matrix system, when the angle  $\theta = 0^{\circ}$ , the fiber surface will be wet very easily [64]. Measurement of the contact angle between the three Nextel 312<sup>TM</sup> fiber samples and the Blackglas<sup>TM</sup> polymer system should indicate to what degree adhesion will develop between the fiber and matrix.

## 3.5 COMPOSITE PERFORMANCE ANALYSIS:

#### 3.5.1 In-situ ESEM processing analysis:

An ElectroScan 2020 environmental scanning electron microscope (ESEM) was used to monitor the polymer-ceramic composite pyrolization to the final CMC state. The cured polymer sample measuring .2 x .2 inches by .196" thick was affixed to the sample crucible with silver filled conductive adhesive. The ESEM was fitted with a hot stage capable of 1000°C and a Nitrogen supply was established. After loading the sample, a slight vacuum of 3-5 torr was established, an operating voltage of 20-25 kv initiated and the nitrogen environment started. The sample was incrementally heated from room temperature to 900°C while micrographs were taken at 100°C intervals and a continuous video was captured. The in-situ pyrolysis procedure was designed to gain further understanding of the various reactions that occur during processing through the polymer to ceramic conversion. Figure

3.2 below summarizes the basic pyrolysis process with associated gas evolution as heat is applied.

During pyrolysis the effect of the mismatch in thermal coefficient between the ceramic fiber and the polymeric matrix creates stresses, which can lead to microcracking. As previously stated, the fiber has a thermal expansion coefficient of  $3.0 \times 10^{-6} \Delta l/l/^{\circ}$ C while the matrix has a varying coefficient as is progresses from a polymer to a ceramic at which time the CTE is  $1.9 \times 10^{-6} \Delta l/l/^{\circ}$ C. In the final ceramic state and after cooling, a residual tensile force would be expected based on expansion coefficient considerations alone, however, the dynamic of matrix shrinkage must also be considered in the pyrolization process.

Along with the inherent fiber-matrix thermal expansion mismatch, the Blackglas<sup>TM</sup> polymer itself has a radical volumetric shrinkage associated with the phase conversion. During the pyrolysis, the shrinkage associated with the conversion from a polymer to an amorphous carbon rich matrix has been known to create matrix cracking and fiber debonding. Due to the magnitude of matrix shrinkage during processing, the effect of CTE mismatch is secondary with respect to that of processing shrinkage. The BN treated, asreceived and desized fiber will be evaluated for their potential interaction with this matrix phenomenon. The ESEM provides the unique possibility to observe the fiber interaction with matrix shrinkage along with the expansion mismatch effects real time.

# PYROLYSIS REACTION

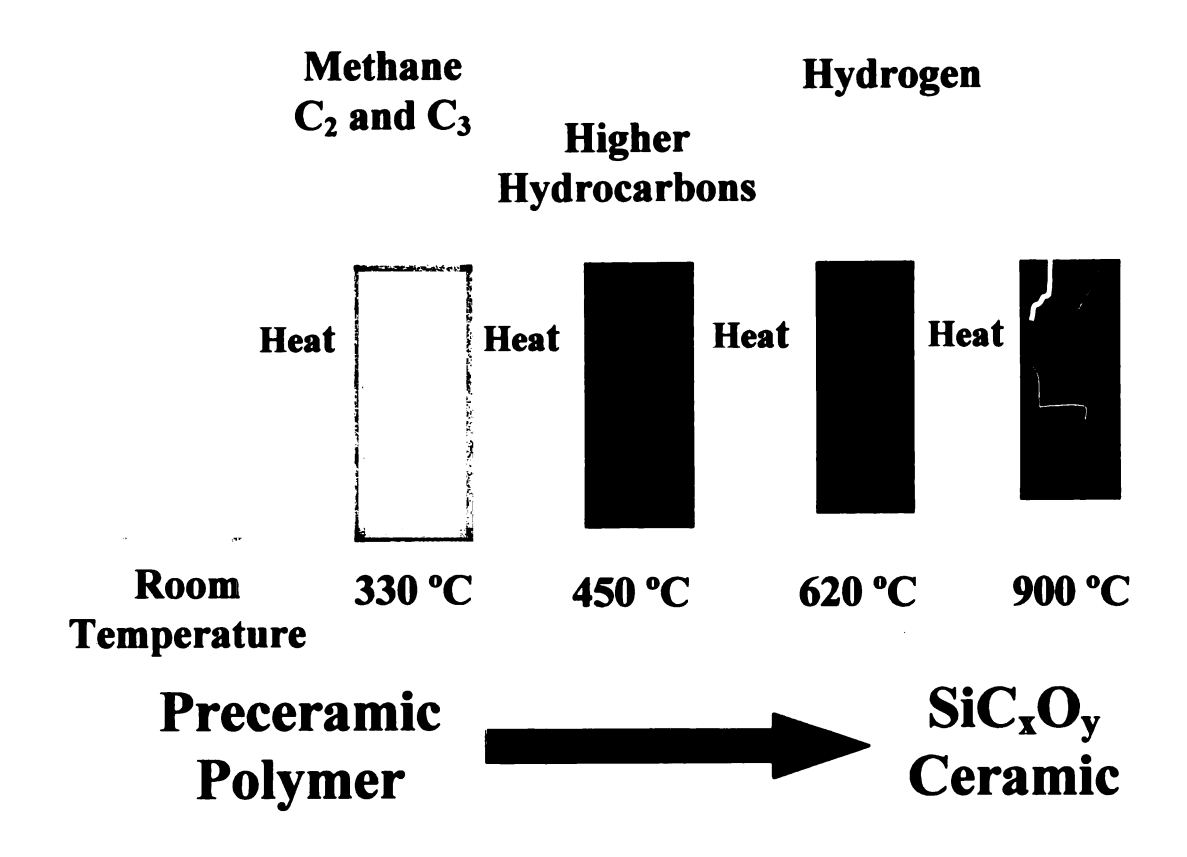


Figure 3.2: Pyrolysis Process.

### 3.5.2 Flexure Testing:

The flexure strength was evaluated in 4-point bending (specimen dimensions: (0.730" x 0.196" x 4", span-to-depth = 16:1) using ASTM standard D790M, 1986. All shear strengths were calculated using standard beam formulae. A minimum of eight specimens was tested in this test configuration. The mean and standard deviation were then calculated. The 4-pt. bend test was performed using a hydraulically driven MTS System 6 load frame with a crosshead speed of 1.27 mm/minute.

## 3.5.3 Short Beam Shear Testing:

The interlaminar shear strength of each composite was determined by testing in short beam shear (specimen dimensions: 0.250" x 0.150" x 2.5", span to depth 4:1) configuration (ASTM D2344 1984). A minimum of 8 specimens was tested in this test configuration. The mean and standard deviation were then calculated. The interlaminar short beam shear tests were performed at Auto-Air Composites, Inc. in Lansing, Michigan on an Instron Corp. Series IX Automated Materials Testing System. The crosshead speed was 1.27 mm/minute.

## 3.5.4 **Iosipescu Testing:**

The in-plane (interlaminar) shear strength (specimen dimensions: 0.75" x 0.196" x 3.5") was determined using the Iosipescu shear test (ASTM D5379/D5379M 1993) with the warp direction in-line with the load direction. A minimum of 8 specimens was tested in this test configuration. The mean and standard deviation were then calculated. The in-plane Iosipescu shear test was performed using a hydraulically driven MTS System 6 load frame with a crosshead speed of 1.27 mm/minute.

#### 3.6 FRACTURE ANALYSIS:

An ElectroScan 2020 environmental scanning electron microscope (ESEM) and a JEOL JSM-6400V SEM were used to examine the surface of failed 4-pt. bend specimens. The JEOL system was equipped with a Noran Vantage System for energy dispersive x-ray spectroscopy (EDX). The EDX system is equipped with a Moxtek window having a lower limit of detection of beryllium with a Noran Extreme detector with a resolution of 126 eV. The fracture analysis of BN treated, as-received and desized flexure samples will be conducted to determine the loci of failure and the corresponding mode of failure. The nature of the failure, whether it is adhesive between either the matrix and fiber or treatment and fiber, cohesive within the matrix, treatment or fiber will provide insight into the ability of the CMC to adsorb energy efficiently.

## Chapter 4

## **RESULTS & DISCUSSION**

## 4.1 Characterization of Fiber Samples:

#### **4.1.1. XPS Results**:

X-ray Photoelectron Spectroscopy (XPS) results (with an error of ±0.5 at.%) are summarized in the table 4.1. The as-received fibers show large carbon, oxygen, and nitrogen concentrations consistent with an organic sizing. Minor amounts of boron, aluminum, and silicon are present with trace amounts of chlorine and sulfur. Since the XPS probing depth is ~6 nm, the presence of boron, aluminum and silicon (fiber constituents) suggest that the sizing may not have uniformly covered the fiber. The XPS results also indicate that desizing the as-received fibers removes much of the nitrogen and carbon, and exposes the oxygen, aluminum, boron and silicon fiber constituents. As expected, the surface chemistry of the desized fibers more closely reflects the chemistry of the aluminoborosilicate fibers. The BN-treated fiber surface composition has 22% C, 21.4% O, 23.4% N, and 21.0% B. Smaller amounts of aluminum and silicon are also present. The results indicate that the boron coating treatment produced a fiber surface rich in boron and nitrogen. The high carbon content probably results from adventitious carbon. No attempts at measuring the BN thickness were made, but the coating thickness is believed to be on the order of 100 to 300 nm [40].

Table 4.1: Fiber Surface Chemistry (atomic%).

As Received	Desized	Boron Nitride Treated
63.9	27.0	22.0
21.0	45.8	21.4
10.7	-	23.4
1.2	5.2	21.0
1.6	18.7	8.1
1.0	3.3	4.2
0.3	-	-
0.3	-	-
	63.9 21.0 10.7 1.2 1.6 1.0 0.3	63.9 27.0 21.0 45.8 10.7 - 1.2 5.2 1.6 18.7 1.0 3.3 0.3 -

Nextel 312<sup>TM</sup> fiber surface morphologies for the as-received, desized and BN-treated samples are shown in figures 4.1, 4.2, and 4.3 respectively. The figures show that each fiber has a slightly different morphology. The organic sizing on the as-received fiber surface appears nonuniform with an uneven thickness. The underlying fiber microstructure is slightly evident. In contrast, the desized fiber shows a uniform microstructure (though individual grains cannot be discerned). The ESEM examination of the BN-treated fiber surface indicated a uniform coverage of coating material.

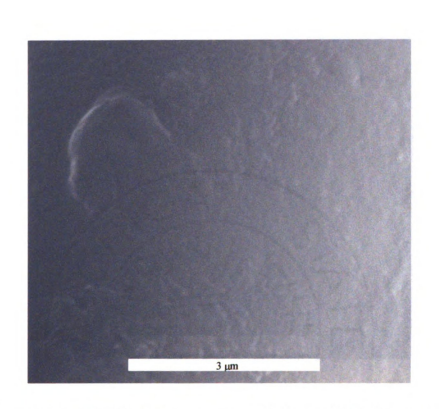


Figure 4.1: ESEM micrograph of as-received Nextel 312™ fiber surface.

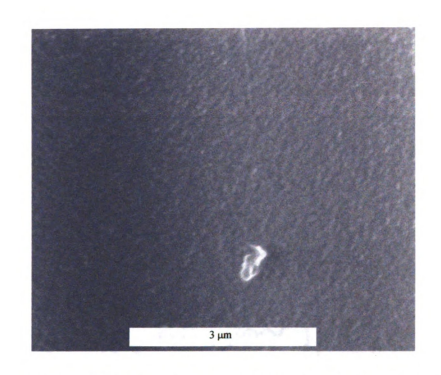


Figure 4.2: ESEM micrograph of desized Nextel 312™ fiber surface.

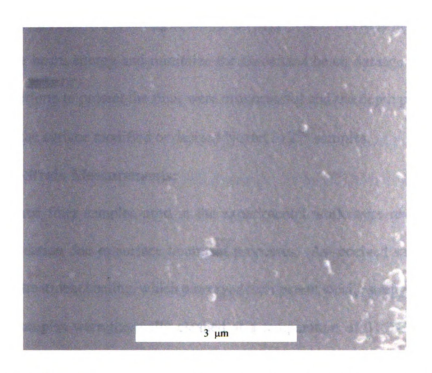


Figure 4.3: ESEM micrograph of BN-treated Nextel 312™ fiber surface.

## **4.1.2** Auger Spectroscopy Results:

Auger Electron Spectroscopy (AES) was used to characterize the single fiber samples surface chemistry and obtain a depth profile of the constituents present. During the analysis of the fibers, it was noted that the insulative capacity of an aluminoborosilicate fiber created a sample charging condition resulting in sample damage. The fibers were gold sputter coated to disperse the beam energy and minimize the associated beam damage incurred by the sample. The efforts to protect the fiber were unsuccessful and the depth profiling was not possible with the surface modified or desized Nextel 312<sup>TM</sup> samples.

### **4.1.3 Stress-Strain Measurements:**

The three fiber samples used in the experimental work were reviewed for their possible degradation due to surface treatment processes. As-received samples were not exposed to pretreatment heating, which preserved their parent tensile strength of 1725 MPa. The desized samples were thermally cleaned at a temperature of 315°C to remove any organic sizing compounds. This low temperature exposure is below any published degradation levels for the Nextel 312<sup>TM</sup> fiber system thereby maintaining the fiber tensile strength of 1725 MPa. The Nextel 312<sup>™</sup> single fiber samples, which were Nitride treated in an ammonia atmosphere at approximately 1150°C to form a BN rich surface composition, were investigated further. The nitriding process required to form the BN layer has been described previously via a reference to the Boeing patented process. Allied Signal has modified this baseline generic process to facilitate Blackglas™ composite performance and the exact parameters of the Nitriding process are proprietary [57]. After the proprietary nitriding process, Allied Signal performed testing of BN treated single fibers in uniaxial tension. The data suggests that the initial fiber tensile strength of 1725 MPa was reduced 710% to 1595 MPa. Tensile property reduction of this nature is believed to be a result of Boria leaching from the bulk fiber structure.

The Blackglas<sup>™</sup> polymer precursor used in this experiment proved extremely brittle after the initial cure and exhibited extensive cracking. Single fiber fragmentation coupons were, therefore, omitted from the testing because the Blackglas<sup>™</sup> ceramic matrix was too brittle for sample preparation and would otherwise not yield the birefringent patterns or photoelastic response necessary to obtain critical fiber lengths required to compute the interfacial shear strength. Polymer state Blackglas<sup>™</sup> encapsulation would reveal little about the interfacial shear stress in the final CMC system and therefore was not considered either. Single fiber testing with the ceramic matrix would yield important data for determining the interfacial shear strength however the microcracking which occurs during processing makes it impossible to process single fibers in with a matrix rich dog bone geometry.

## **4.2 Composite Sample Processing Results:**

Several reports have studied the pyrolytic conversion of polysilsequioxanes to silicon oxycarbides [65]. These studies indicate that pyrolyzing a polysiloxane polymer produces silicon oxycarbide with a high ceramic yield (70-80 wt%) containing a network of microcracks and porosity due to volume shrinkage (55%). The amount of microcracking and porosity increases when fabricating a silicon oxycarbide\aluminoborosilicate fiber composite due to fiber constraints and the dissimilar shrinkage between the matrix and fibers [66,67]. Thus several infiltration cycles are required to fill the cracks and densify the matrix of the composite.

The processing data in Figure 4.4 shows the % weight change —relative to the composite after one pyrolization cycle, but with no impregnation of resin (BG(0))—as a

function of infiltration cycle for as-received and BN-treated fiber composites (no statistical difference between the two types of composites was measured). The green composite consists of 58-wt% fiber ( $\rho = 2.7$  gm/ml) and 42-wt% resin ( $\rho = 1.1$  gm/ml). The first pyrolysis cycle going from the cured state to the BG(0) is the most important step since this determines not only the number of subsequent infiltration/densification and pyrolysis steps to follow, but also the microstructure and properties of the final composite. On the first pyrolysis step, the green compact experiences a 7.1% weight loss and an increase in density. The weight loss results when chemical reactions produce gases (hydrogen and hydrocarbon) that evolve from the polymer [68]. Fortunately, much of the porosity present after BG(0) is interconnected and will be filled with resin on subsequent infiltrations.

On subsequent pyrolysis cycles, the composites gain weight. The most dramatic weight gain occurs after the second pyrolization (BG(1)) where a 15.6% gain is observed. Less dramatic increases are observed for subsequent pyrolization/infiltration cycles. The total weight gain in the fifth impregnation was 33.3%. After five infiltrations the apparent (or open) porosity (the extent of the closed porosity is unknown) did not change suggesting that the maximum densification, using the current procedure, had been reached. As Rangarajan et al. points out, this method of silicon oxycarbide matrix composite fabrication leads to closed porosity in the form of micro- and nano-sized pores [67].

Conversion of the pre-ceramic polymer (without fibers) to silicon oxycarbide was also monitored. The volume decreased to 55% of the initial volume. The typical composition of the silicon oxycarbide glass, as determined by XPS, was 24 wt% carbon, 47 wt% silicon, 28 wt% oxygen, <0.4 wt% hydrogen and <0.1 wt% nitrogen. This composition results in a matrix composition of SiC 1.21O1.06. The matrix char yield after pyrolysis was 81 to 86% and

the density increased from 1.10 gm/ml (polymer) to 2.11 gm/ml (ceramic). The surface chemistry of the ceramic matrix material was measured and consisted of 17.6 at.% carbon, 38.4 at.% oxygen, and 44 at.% silicon. No evidence of nitrogen, which is present as a gas during the pyrolization process, was detected in the matrix material.

Attempts at fabricating composites with desized fibers were unsuccessful due to spontaneous delamination of the fiber and matrix plies after each pyrolization cycle. The exact cause of the delamination is not known; however, a strong fiber-matrix chemical reaction combined with resin shrinkage and differences in matrix and fiber coefficient of thermal expansion (CTE) can lead to high residual stresses causing delamination [69].

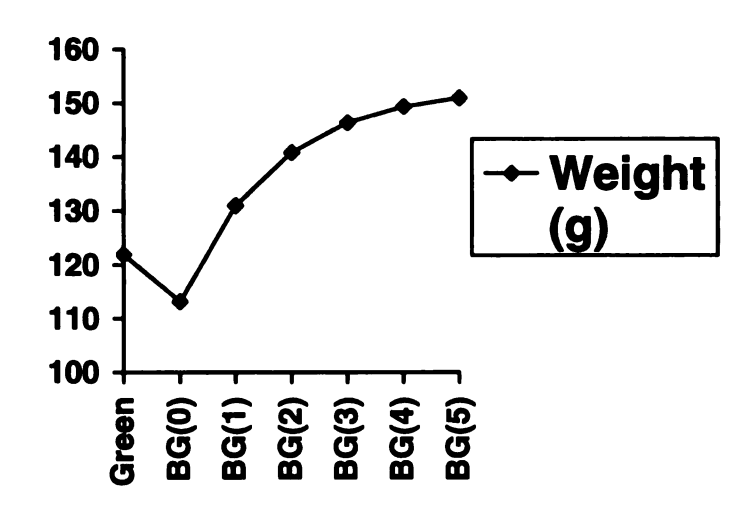


Figure 4.4: Typical weight gain curve through densification process.

Table 4.2: Sample Weight Gain Through Densification Cycles.

Process Stage	Weight (g)	Cumulative weight gain%	Percent Delta	Thickness (in.)
Green	121.91	***	***	.1490
BG(0)	113.21	100	-7.13	.1480
BG(1)	130.93	115.64	15.64	.1424
BG(2)	140.79	124.35	7.53	.1412
BG(3)	146.34	129.25	3.94	.1405
BG(4)	149.28	131.85	2.01	.1405
BG(5)	150.98	133.35	1.14	.1405

# 4.3 ADHESION MEASUREMENTS:

# 4.3.1 Interfacial Testing System:

The microindentation technique test measures the fiber-matrix interfacial shear strength (IFSS) of an individual fiber. The microindentation test consists of loading the cross-section of an individual fiber oriented normal to the polished surface with a conical indenter. The load is incrementally applied until a crack (debonding) develops at the fiber/matrix interface. Reference Figure 4.5 and Figure 4.6 for typical debonding indications about fiber circumference. The load at debonding is assumed to represent the shear strength of the interface. The debonding load is influenced not only by the fiber/matrix bond strength but also by the fiber and matrix properties (such as moduli and Poisson's ratios) and fiber packing. An analytical closed form solution for the stress distribution around the indented fiber is not available so the calculation of an average shear stress relies on a finite element calculation [70]. The data reduction scheme uses the following formula:

IFSS = 
$$A \frac{f_g}{d_f} \left[ 0.875696 \sqrt{\frac{G_m}{E_f}} - 0.018626 \ln \left( \frac{d_n}{d_f} \right) - 0.026496 \right]$$

Where  $f_g$  is the load at debonding,  $G_m$  is the shear modulus of the matrix,  $E_f$  is the tensile modulus of the fiber,  $d_n$  is the distance between the nearest fiber and the loaded fiber,  $d_f$  is the diameter of the fiber, and A is a conversion factor. For the silicon oxycarbide matrix,  $G_m = 73.75$  MPa, and v = 0.28. The fiber tensile modulus is 138 GPa, with a tensile strength of 1.7 GPa.

The IFSS results are for the as-received and BN-treated fiber composites are reported in Table 4.3. For the as-received fiber composite, the IFSS was found to be  $8.9 \pm 2.1$  GPa. This stress level exceeds the fracture strength of the fiber and the fracture stress of the silicon

oxycarbide. Tested fibers that exhibited cracking were discarded and not used in the calculation of the IFSS average. The anomalously high value of IFSS results because the FEM model does not include residual stresses caused by the radial shrinkage stress of the matrix around the fiber or the longitudinal compression of the fiber caused by matrix shrinkage. These residual stresses in the as-received fiber composite could be extremely high. The effect of fiber spacing can also have important consequences on the debond strength (less for high modulus materials). This certainly will affect the outcome somewhat, but not enough to alter the conclusion: the IFSS of the as-received fiber composite is very high.

The data in Table 4.3 for the IFSS of the BN-treated fiber composite is  $860 \pm 34$  MPa. Experimentally, the tested fibers debonded gently and clearly showed interfacial crack formation. The standard deviation is 4.0% of the mean value. This level of uncertainty could result from several factors including: the testing of fibers from different regions of the composite (differences in the thermal residual stresses of the innermost and outermost plies could affect debond strength) [71].

Table 4.3: Interfacial Shear Strength Results.

Sample	Strength	Strength
_	(MPa)	(ksi)
BN treated	860 ± 34	125 ± 4.9
As received	$8860 \pm 2090 \qquad 1289 \pm 305$	
Desized	Samples delaminated during processing.	

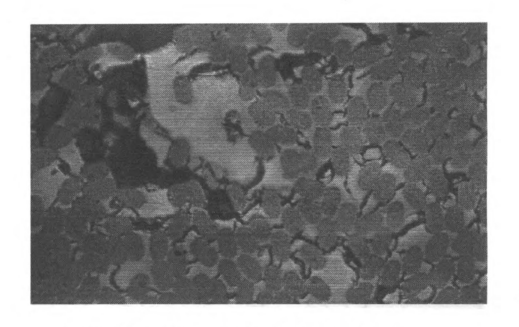


Figure 4.5: IFSS micrograph of as-received sample.

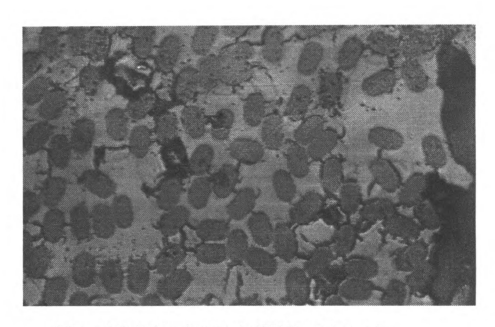


Figure 4.6: IFSS micrograph of BN treated sample.

#### **4.3.2** Fiber Pull-Out Test:

The fiber pull-out test was not completed due to the sample fabrication difficulty encountered with this matrix-fiber combination. A single fiber could not be cast in the matrix material due to matrix cracking and specimen instability. The cured polymer exhibits visible macrocracking and the pyrolyzed polymer features 55% volumetric loss during processing to 900°C (1652°F). In order to complete the pull out test, the matrix must be uniformly fixtured while the fiber is placed in uniaxial tension, which could not be achieved with the 493 Blackglas™ ceramic matrix system.

# 4.3.3 Wettability

The Blackglas<sup>TM</sup> polymer resin system 493A was utilized in the fabrication of all composite panels. The resin system has been designed for ease of wet laminating practices and RTM (resin transfer molding) process, in that the viscosity is extremely low. The viscosity measures 5 centipoise, which enables the resin to permeate the fiber preform or fabric lay up as the application dictates. During fabrication evaluations, the resin was easily infused into the fabric with no noticeable air bubbles generated as the fabric was saturated. Typically, air bubbles are generated when a high viscosity system is forced into the reinforcement as entrapped air attempts to exit the layup. The spontaneous wet out of the fabric was a clear indication that the wettability as observed was very good and that surface tension issues have little effect on the resin to adhere to the fiber system.

#### 4.4 COMPOSITE PERFORMANCE ANALYSIS:

# 4.4.1 In-Situ ESEM Processing Analysis:

The polymer to ceramic conversion was observed real time via an ElectroScan 2020 environmental scanning electron microscope equipped with a hot stage and nitrogen environment. The instrument was operated at 20-25 kv while evacuated at 3-5 torr. 2-D composite panels which were previously polymer cured were sectioned into .2 inch square by .196 inch thick test pieces. Individual cycles were run for the as-receives-desized and BN treated samples. Samples were heated from room temperature to 900°C in order to reproduce the conversion process and witness the contribution of the three different fiber surfaces. Micrographs, Figure 4.7 through Figure 4.12, were taken at RT-161°C, 301-327°C, 500°C, 600°C and 900°C respectively. The temperatures were selected due the process milestones as shown in Figure 3.2 that illustrates the various byproducts throughout the conversion process with corresponding temperatures.

The initial micrographs that were taken at RT-161°C serve as a baseline image where no apparent changes in the structure were perceivable. At this initial stage there is evidence of fiber debonding and matrix cracking in all three samples. The polymer had, during the initial cure and subsequent cooling, experienced cracking due to shrinkage inherent to the curing process. Neat polymer resin samples had displayed evidence of cracking after initial polymer cure, which indicates the initial cracks witnessed at RT-161°C were not created solely from fiber-matrix thermal expansion mismatch.

Micrographs taken at 301-327°C indicate some enhanced signs of cracking in both the matrix and about the fiber circumference. This temperature range is that which begins the evolution of methane  $C_2 + C_3$  gases and also where volumetric shrinkage of the matrix

occurs. The as-received and desized samples appear to have a higher frequency of matrix (fiber to fiber) cracks while the BN treated sample reveals more pronounced fiber debonding.

Increasing the temperature to 500°C begins the release of higher hydrocarbons and further matrix shrinking. In both the as-received and desized samples further widening of the matrix cracks is evident which could be attributed to adhesion of the fiber to the matrix which drives the volumetric shrinkage forces within the sample to relieve themselves via macrocracking within the matrix. The BN treated samples, however, have a different appearance as the fibers appear to unbond more discretely leaving the matrix more in tact in comparison the other samples. The BN treated sample appears to have fibers debonding and pushing out of the sample surface which again could be a result of the coupon attempting to relieve stresses built in the matrix due to the volumetric shrinkage.

Samples elevated to 600°C are beginning to evolve hydrogen gases and continue to crack both within the matrix and around individual fibers. The as-received samples show signs of fiber debonding as the fibers appear to be moving in and out of the surface. The desized sample reveals more widened matrix cracking and a lesser degree of fiber unbonding. The BN sample continues to displace fibers along their axis as slippage and debonding occurs.

The final pyrolysis temperature of 900°C continues with hydrogen evolution and completes the matrix shrinkage of 55% and associated density increase from 1.09 g/cm³ to 2.2 g/cm³. The adhesion between the Nextel 312™ fiber and the Blackglas™ matrix appears to be generally in tact while the as received sample demonstrates smaller matrix cracks and evidence of more localized unbonding around individual fibers. This more incremental mechanism to relieve internal processing stresses, may be the reason the as-received samples

remain intact while the desized sample were completely delaminated to the state where further testing was not possible. The as-received samples were coated with an organic coating which most probably decomposed to form a thin layer of carbon as the samples were processed. The carbon boundary layer may have, in an inert atmosphere such as Nitrogen, provided the necessary decoupling path that the composite relieved process stresses more gracefully and did not delaminate, as did the desized sample. The BN treated sample appears to unbond consistently throughout the processing stages as was evidenced by the large in and out of plane displacements made by individual fibers. It would seem then that a mechanism to relieve internal stresses must be provided to prevent the composite from delaminating and preventing subsequent infiltration processing.

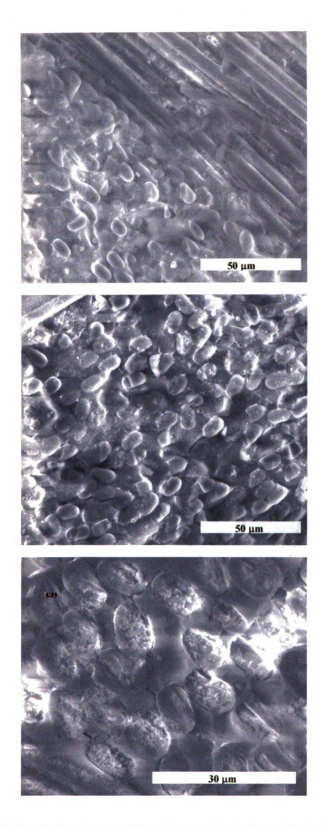


Figure 4.7: ESEM in-situ pyrolysis. Top: As Received fiber composite at 650X and room temperature. Middle: Desized fiber composite at 650X and Room temperature. Bottom: BN Treated fiber composite at 1500X and 161°C.

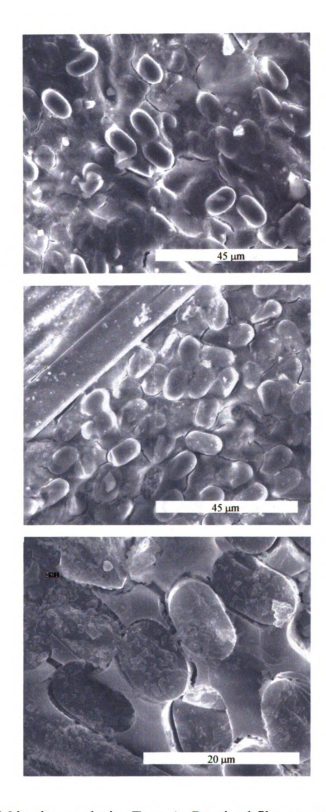


Figure 4.8: ESEM in-situ pyrolysis. Top: As Received fiber composite at 1000X and 300°C. Middle: Desized fiber composite at 1000X and 301°C. Bottom: BN Treated fiber composite at 2500X and 327°C.

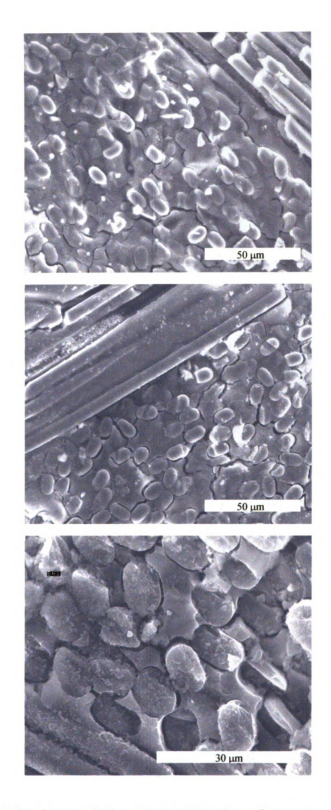


Figure 4.9: ESEM in-situ pyrolysis. Top: As Received fiber composite at 600X and 501°C. Middle: Desized fiber composite at 500X and 500°C. Bottom: BN Treated fiber composite at 1500X and 499°C.

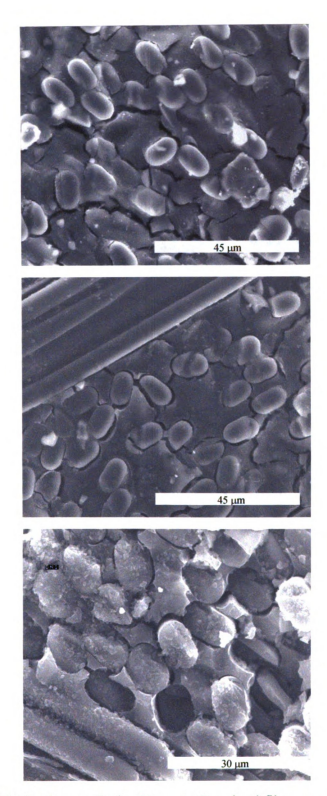


Figure 4.10: ESEM in-situ pyrolysis. Top: As Received fiber composite at 1000X and 599°C. Middle: Desized fiber composite at 1000X and 600°C. Bottom: BN Treated fiber composite at 1500X and 600°C.

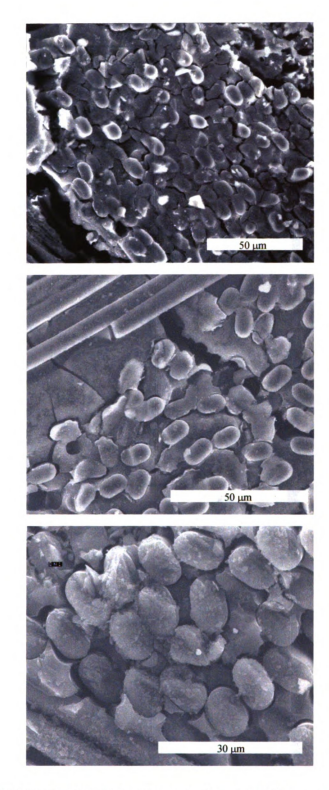


Figure 4.11: ESEM in-situ pyrolysis. Top: As Received fiber composite at 600X and 900°C. Middle: Desized fiber composite at 850X and 900°C. Bottom: BN Treated fiber composite at 1500X and 900°C.

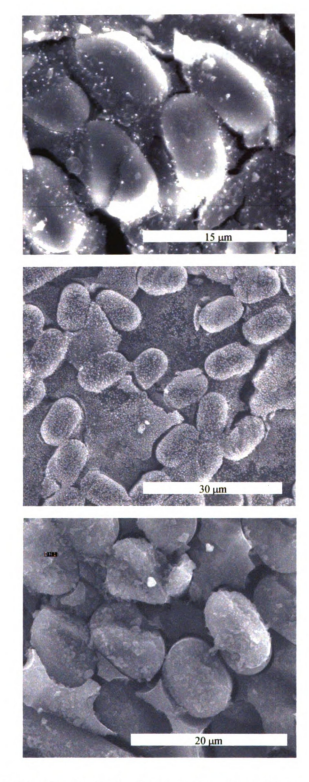


Figure 4.12: ESEM in-situ pyrolysis. Top: As Received fiber composite at 3050X and 900°C. Middle: Desized fiber composite at 1500X and 1000°C. Bottom: BN Treated fiber composite at 2500X and 901°C.

#### 4.4.2 Flexure Data:

The flexural strength is equal to the maximum stress in the outer surface at the moment of break. As Table 4.4 and Table 4.5 indicate, the flexural strength of the BN-coated composite was 178.2 MPa versus 25.3 MPa for the as-received composite. In addition, the strain-to-failure was less than 0.05% for the as-received fiber composite and 0.5% for the BN-coated fiber composite. Increases of ~700% in flexural strength and ~1000% in the strain- to-failure suggests that the BN-coated fiber composites are stronger and tougher in flexure than the as-received fiber composites. Load-displacement data shown in figure 4.13 illustrates relative strain capabilities. The strength of the BN-coated fiber composites agree with the flexural strengths reported by Zhao et al. [72]. At ultimate strength, both of the composites failed on the tensile stress side. The low values of strength observed for the as-received composites are close to that reported for the matrix material alone and suggests that the Blackglas<sup>TM</sup> matrix and not fiber/matrix interface debonding is playing the dominant role in determining the ultimate strength.

Table 4.4: As-Received Flexure Strength

Sample I.D.	Maximum Stress (psi)	Maximum Stress (MPa)
ARFlex 1	3049	21
ARFlex 2	3794	26
ARFlex 3	3889	27
ARFlex 4	4315	30
ARFlex 5	4148	29
ARFlex 6	3898	27
ARFlex 7	3264	23
ARFlex 8	3144	22
Mean:	3688	25
S.D.:	476	3

Table 4.5: BN Treated Flexure Strength

Sample I.D.	Maximum Stress (psi)	Maximum Stress (MPa)
BNFlex 1	Not Tested	Not Tested
BNFlex 2	24966	172
BNFlex 3	26633	184
BNFlex 4	25999	179
BNFlex 5	25202	174
BNFlex 6	24479	169
BNFlex 7	27137	187
BNFlex 8	27064	187
BNFlex 9	25969	179
Mean:	25935	179
S.D.:	992	7

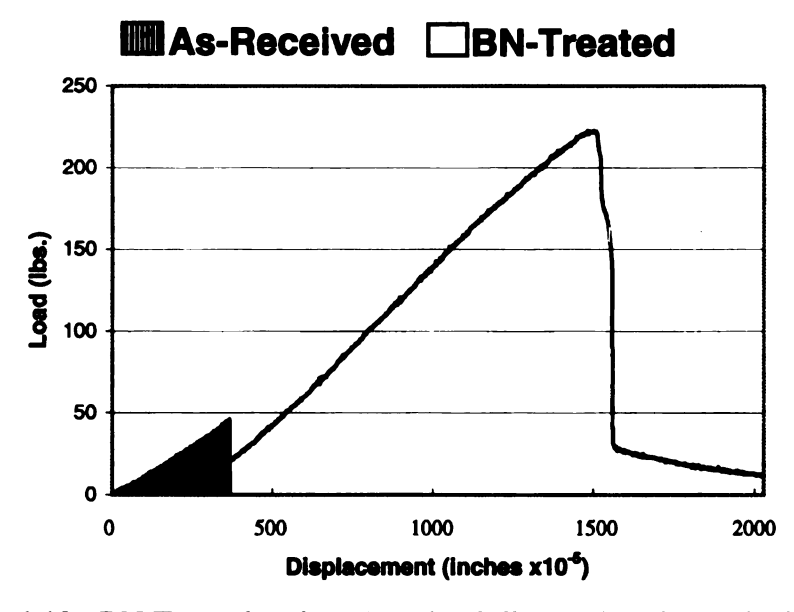


Figure 4.13: BN Treated and As-Received Flexure Load vs. Displacement.
Illustrating .05% strain to failure for as received and .5% for the BN treated flexure samples.

#### 4.4.3 Short Beam Data:

The data in Table 4.6 and Table 4.7 also indicates that BN-treated fibers show a 600% increase in the interlaminar shear strength as determined using the short beam shear test.

Low values of interlaminar shear suggest that the matrix properties are playing the major role in determining the shear strength of the composite.

Table 4.6: BN Treated Short Beam Shear Strength

Sample I.D.	Interlaminar Shear (psi)	Interlaminar Shear (MPa)
BNSBS 1	4658	32
BNSBS 2	4711	32
BNSBS 3	4756	33
BNSBS 4	4777	33
BNSBS 5	4607	32
BNSBS 6	4569	32
BNSBS 7	4328	30
BNSBS 8	4731	33
BNSBS 9	4799	33
BNSBS 10	4685	32
Mean:	4662	32
S.D.:	138	1

Table 4.7: As-Received Short Beam Shear Strength

Sample I.D.	Interlaminar Shear (psi)	Interlaminar Shear (MPa)
ARSBS 1	752	5
ARSBS 2	770	5
ARSBS 3	816	6
ARSBS 4	773	5
ARSBS 5	708	5
ARSBS 6	740	5
ARSBS 7	698	5
ARSBS 8	700	5
Mean:	745	5
S.D.:	42	0

# 4.4.4 Iosipescu In-Plane Shear Strength:

The data in Table 4.8 and Table 4.9 shows the as-received fiber composite has inplane shear strength of 9 MPa, while the BN-treated composite has shear strength of 102
MPa. This represents a ~1000% increase in the interlaminar shear strength when the
composite is fabricated using BN-treated fibers. In addition to differences in the shear
strength, the as-received fiber composite failed when cracks developed and propagated in
straight-lines perpendicular to the loading direction and between the notches. On the other
hand, the BN-treated fiber composite failed with cracks developing and propagating between
the notches along a line approximately 45° to the loading direction. Macroscopically, the
BN-treated fiber composites had some fiber pull-out, while the as-received fiber composites
had smooth, flat surfaces.

Table 4.8: As-Received Iosipescu In-Plane Shear Strength

Sample I.D.	Maximum Shear Stress (psi)	Maximum Shear Stress (MPa)
AR 1	2552	18
AR 2	250	2
AR 3	333	2
AR 4	2274	16
AR 5	259	2
AR 6	1940	13
AR 7	445	3
AR 8	2124	15
AR 9	2911	20
AR 10	280	2
Mean:	1337	9
S.D.:	1110	8

Table 4.9: BN Treated Iosipescu In-Plane Shear Strength

Sample I.D.	Maximum Shear Stress (psi)	Maximum Shear Stress (MPa)
BN 1	14382	99
BN 2	15762	109
BN 3	11307	78
BN 4	15615	108
BN 5	12681	87
BN 6	14359	99
BN 7	17204	119
BN 8	16366	113
BN 9	16305	112
BN 10	13819	95
Mean:	14780	102
S.D.:	1829	13

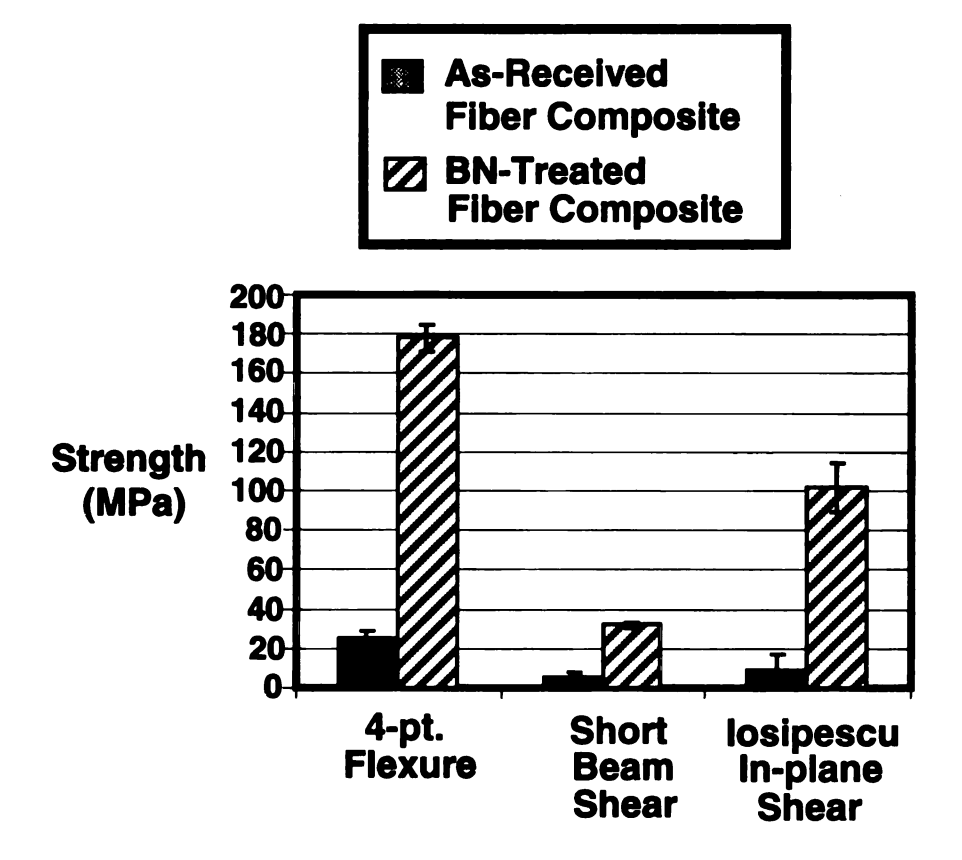


Figure 4.14: Mechanical Testing Summary

Both types of observed failure modes are generally acceptable; however, the large standard deviation of the as-received fiber composites indicates a large amount of scatter in the individual tests. Of the ten tests, five of the test values were at or below 3 MPa, while the other five test values were above 13 MPa. If the 5 test values at 3 MPa and below are disregarded, the average shear strength is  $16.4 \pm 2.7$  MPa. This is still significantly below the value of 102 MPa for the BN-treated fiber composite, but with a much smaller standard deviation. The reason(s) for the large amount of scatter in the as-received fiber composites is unknown, though one possible contribution to the observed scatter in the shear strength could be the nonuniformity of the organic sizing. If during repeated infiltrations the sizing is consumed, regions of the as-received fibers will behave similar to desized fibers. The desized regions would generate large stress concentrations and cause the composite to fail at a lower stress level. Another possibility is the presence of small, unobservable, composite manufacturing flaws or small cracks introduced in when machining the notches. Regardless of the origin, the differences in shear strength between the as-received fiber composite and the BN-treated fiber composite is substantial.

The summary data provided in Figure 4.14 illustrates the significant improvement gained when the Boron Nitride system is utilized. The BN treatment also provided a more predictable failure as demonstrated through the lower standard deviations noted.

#### 4.5 FRACTURE ANALYSIS:

The fracture properties of ceramic matrix composites are governed by matrix cracking followed by interaction of cracks with the fibers and interfaces. Within the composite, energy dissipative processes such as fiber-matrix debonding, crack bridging, fiber pull-out, multiple

crack formation and crack deflection can be observed [73]. To determine the fiber-matrix damage and fracture process for each composite type, specimens failed in 4-point flexural tests were examined. In all cases, during mechanical testing, cracking sounds were heard near the failure load, but no visual indication of failure was observed until catastrophic failure.

The ESEM micrographs in Figure 4.15a and Figure 4.15b show the interlaminar fracture surfaces of desized fiber composites. Figure 4.15a is a low magnification view showing matrix cracking caused by resin shrinkage. The large cracks seen in the matrix are indicative of a weak matrix, a consequence of the dissimilar shrinkage of fiber and matrix during pyrolysis and cool down from temperature. A higher magnification in Figure 4.15b shows how the crack propagated near the fiber surface. This is consistent with XPS results that indicated delamination cracks propagated through the matrix and that the locus of failure was cohesive in the matrix.

The micrographs shown in Figure 4.16a and Figure 4.16b illustrate of the failure behavior of as-received fiber composites. Figure 4.16a shows a macroscopically rough surface indicating some crack deflection as it passed through the composite. A higher magnification view shown in Figure 4.16b indicates a microscopically smooth surface with no evidence of hackles or scallops or fiber pull-out. In particular, the crack path shows a smooth transition across the fiber-matrix interface. These observations indicate strong fiber-matrix adhesion. This also explains why the composite properties of flexural and shear strength are dominated by the mechanical properties of the matrix. These results are consistent with the XPS examination of the fracture surface chemistry that indicates exposed fiber surfaces. These results suggest that the locus of failure alternates between the fiber-

matrix interface and cohesive failure of the matrix. The high magnification view also shows the presence of small voids and microcracks at some of the fiber- matrix interfaces.

ESEM micrographs of BN-treated fiber composite fracture specimens are shown in Figure 4.17a and Figure 4.17b. The fracture surfaces seen here are significantly different than either the desized or the as-received fiber composites. Figure 4.17a shows that macroscopically the fracture surfaces are extremely rough with a substantial amount of fiber pull-out. In addition, fiber fracture continues at various planes throughout the composite, resulting in a brush-like rough surface of broken fibers and/or bundles. At a higher magnification fiber-matrix separation is observed and resin fracture occurs between fibers. In this case, as Figure 4.17b shows, fiber pull-out results in a cupping surface. The presence of a large amount of matrix debris suggests a large amount of energy dissipation during crack propagation through the composite. These failure surface observations correlate well with the mechanical properties. Crack propagation by debonding the fiber- matrix interface is typical throughout the crack-propagation path for the higher strength sample. This type of cracking consumes more energy and makes other energy dissipating mechanisms, such as fiber pullout, fiber bridging, and crack deflections, possible. The amount and extent of fiber/matrix debonding give an indication of how well the energy-dissipating mechanisms perform. The extensive debonding along the crack propagation path can be attributed to the relatively homogeneous distribution of the fibers and matrix, which makes extensive fiber pullout and fiber bridging possible.



Figure 4.15a: Delaminated desized composite sample at low magnification.



Figure 4.15 b: Delaminated desized composite sample at high magnification.

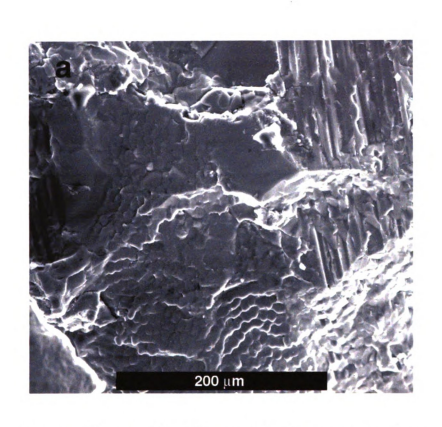


Figure 4.16a: As received low magnification fracture surface.

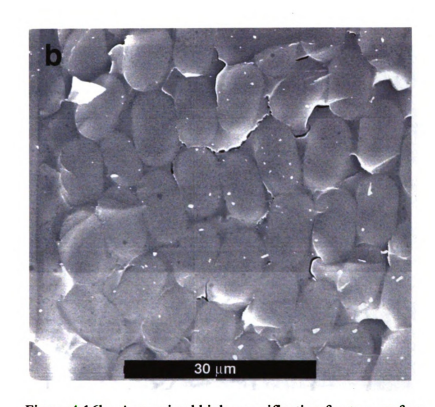


Figure 4.16b: As received high magnification fracture surface.

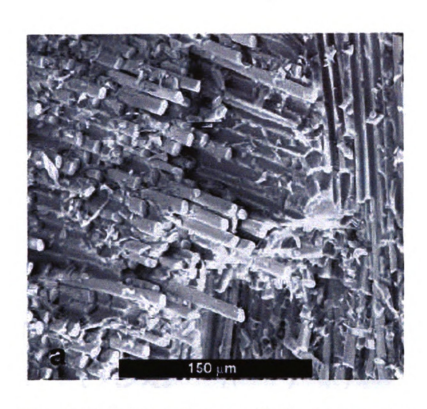


Figure 4.17a: BN treated low magnification fracture surface.

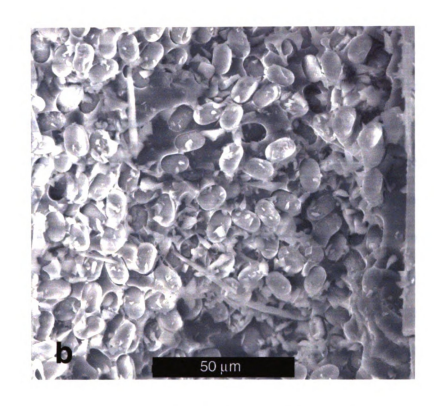


Figure 4.17b: BN treated high magnification fracture surface.

#### 4.6 SURFACE CHEMISTRY OF FRACTURED SPECIMENS:

Controlling the fiber-matrix interface behavior is a key factor in developing appropriate mechanical properties of composites. Determination of the locus of failure at the fiber- matrix interface provides direct information on how the fiber coating affects the load transfer from the matrix to the fiber. As the diagram in Figure 4.18 shows, for the case of silicon oxycarbide composited with BN treated aluminosilicate fibers, failure can occur (1) cohesively in the matrix, (2) at the matrix-coating interface, (3) at the coating- fiber interface, (4) cohesively in the matrix, or (5) cohesively in the BN coating. To help determine the locus of failure, XPS analysis of as-received, desized and BN-coated composite specimens fractured in 4-point bend tests (or delaminated) was performed and the results are reported in Table 4.10. Since the sampled area is approximately 2 mm<sup>2</sup>, the XPS data are averaged over a large spatial area and accumulated from fiber surfaces, fiber ends, and matrix material. The large sampling area makes a definitive identification of the locus of failure difficult, but does provide useful information that can help guide the determination.

Data for the spontaneously delaminated desized fiber composites indicates the presence of carbon, oxygen and silicon. The lack of an aluminum signal suggests complete coverage of the fibers by matrix material and cohesive failure of the matrix near the fiber surfaces. The as-received fiber composite shows large amounts of carbon, oxygen and silicon, with small amounts of nitrogen, boron and aluminum. In contrast to the desized fiber composites, small amounts of aluminum, nitrogen and boron are seen in the as-received fiber composites. This suggests that at least some exposed fiber surface is being detected. Though the locus of failure for the as-received composite cannot be made with certainty, differences between the desized and as-received composites suggest differing loci of failure.

The composition of the BN-treated fiber composite listed in Table 4.10 indicates a large amount of boron and nitrogen in a 1:1 correspondence. In addition, a small oxygen concentration was measured. These results suggest that the BN coating covers the surface of the fiber and excludes the aluminum in the fiber from being probed by the x-ray. Since XPS analysis of 4 pt. flexure specimens is suggestive, but inconclusive in determining if the fiber-matrix locus of failure occurred at the fiber-BN interface or the BN- matrix interface, EDX analysis of the fracture surface was performed.

EDX was used to analyze the BN-coated fiber surfaces exposed during the fracture process and the matrix material (fiber channels) exposed during fiber pull-out. (Note that because of the inherent surface roughness of the fracture surfaces extreme care was taken to acquire accurate EDX spectra of the convex fiber and concave channel surfaces.) Figures 4.19a and 4.19b show an EDX spectrum taken from a region of the fracture surface where fiber pull-out (channel) occurred. No evidence of boron (0.185 keV) is seen in the spectra, though nitrogen (0.392) is clearly evident. The nitrogen signal could result from nitrogen atoms incorporated into the matrix during composite fabrication (though nitrogen was not detected in the XPS analysis of the matrix, the sampling depth of XPS is much less (2 µm compared to 6 nm) than EDX) or could be remnants from the BN coating. An EDX spectrum taken from the fiber surface is shown in Figures 4.20a and 4.20b. The EDX spectrum shows boron and nitrogen on the fiber surface. The EDX results, combined with the XPS results, indicate the locus of failure of BN-coated fiber composites occurs primarily at the BNmatrix interface. The possibility of failure within the BN coating cannot be completely eliminated; however, the data suggests that the majority of the coating remains on the fiber surface. This result indicates that the thin BN coating forms a stronger bond with the fiber than the matrix, and has enough BN-matrix bond strength to provide load transfer, yet weak enough to allow fiber pullout during crack propagation.

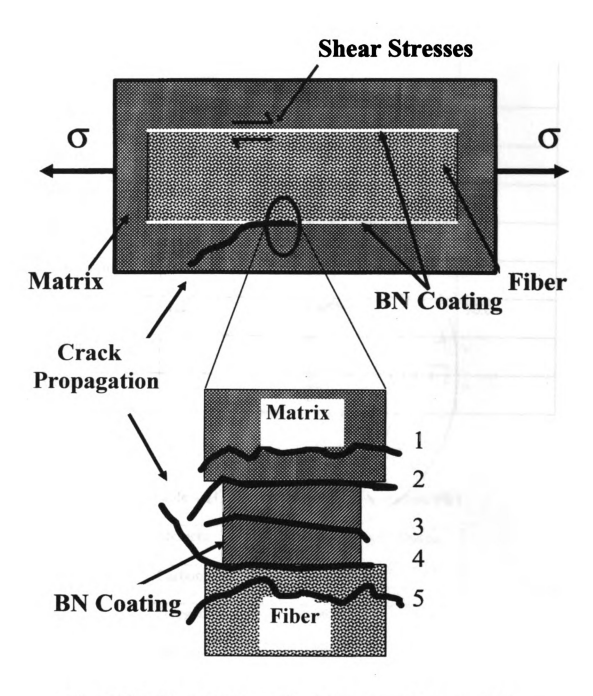


Figure 4.18: Schematic diagram illustrating the possible locus of failure.

Table 4.10: Fracture Surface Atomic Concentrations (%)

Element	Boron Nitride	As Received	Desized
	Treated		
Carbon	58.1	52.4	52.8
Oxygen	18.0	28.4	31.3
Nitrogen	8.1	0.8	-
Boron	7.9	0.8	-
Aluminum	0.6	3.4	-
Silicon	7.2	14.2	16.0
Sulfur	-	-	-
Chlorine	-	-	

Table 4.11: Matrix Atomic Concentrations (%)

Element	Blackglas™ Matrix
Carbon	17.6
Oxygen	38.4
Silicon	44.0

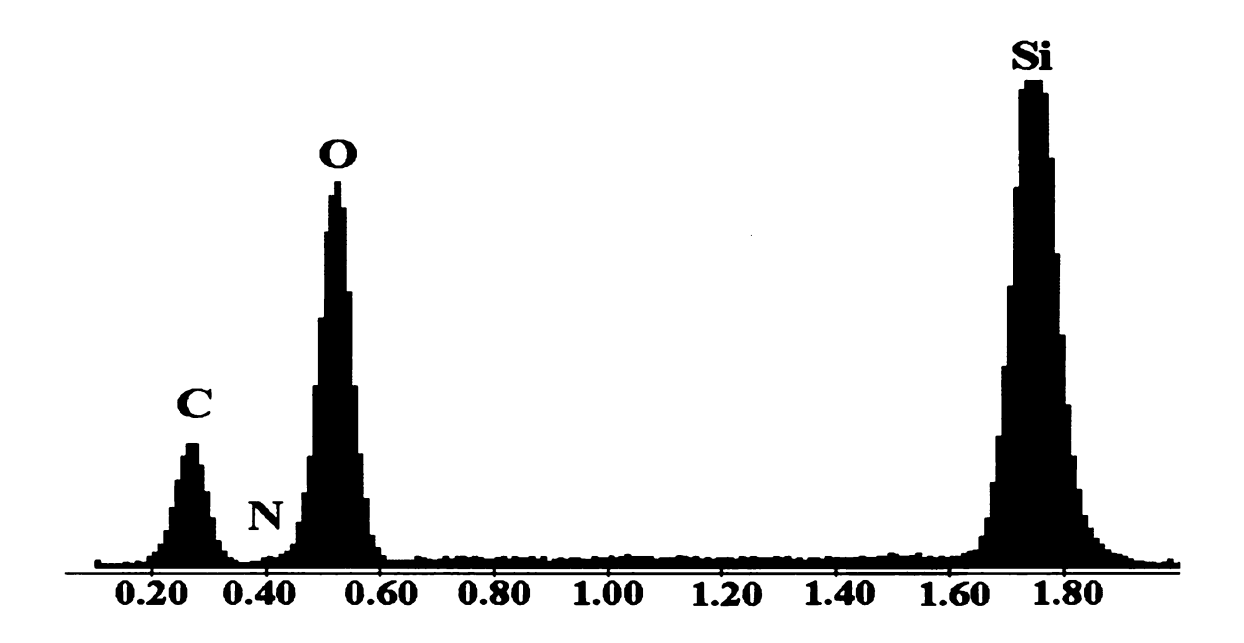


Figure 4.19a

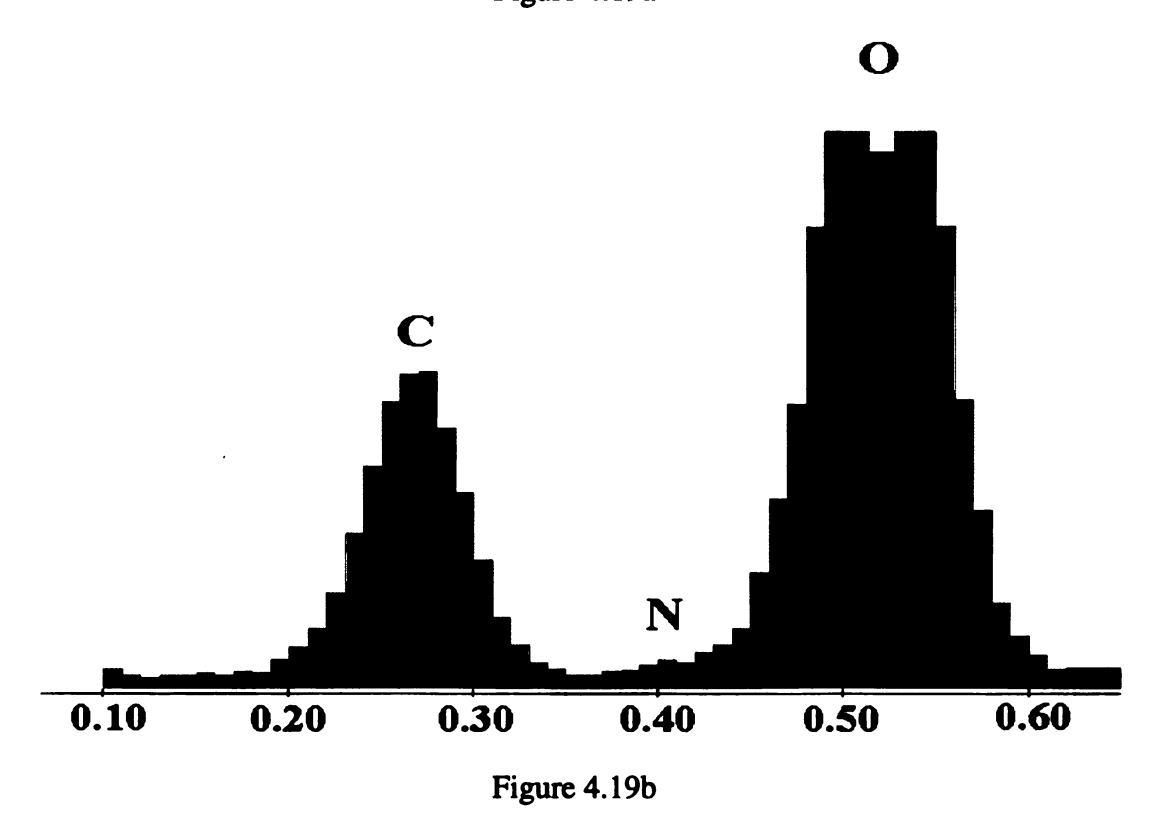


Figure 4.19: EDX spectra taken from the matrix region exposed during fiber pull-out (4.19a) and an enlargement of the low energy section of (4.19a) shown in (4.19b).

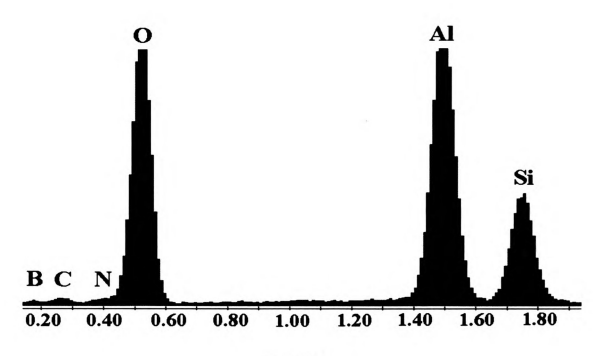


Figure 4.20a

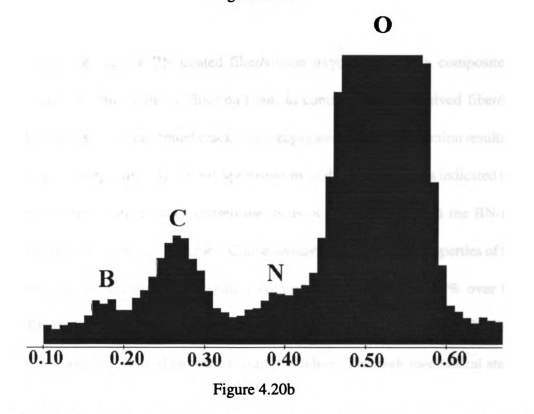


Figure 4.20: (4.20a) EDX spectra taken from the fiber surface showing the presence of boron and nitrogen and 4.20b and enlargement of the low energy spectra shown in 4.20a.

# **Chapter 5**

# **Conclusions**

This work investigates the effects of a boron nitride coating on the mechanical properties of an aluminoborosilicate fiber/silicon oxycarbide composite. The mechanical, chemical, and fracture properties of composites fabricated with BN treated, desized and asreceived fibers are compared. Large internal stresses formed during infiltration/pyrolization of the desized fiber/silicon oxycarbide composite caused the composite to spontaneously delaminate. Fractographic examinations of flexure test specimens indicate that the BN treated fiber/silicon oxycarbide matrix composite has a brush-like surface with extensive fiber pull-out. In contrast, the as-received fiber/silicon oxycarbide composite demonstrated cracks that propagate with little deflection resulting in a smooth surface. Energy dispersive x-ray spectroscopy of the failed surfaces indicated that the presence of the BN coating which caused the locus of failure to occur at the BN-treated fiber/silicon oxycarbide matrix interface. Consequently, the mechanical properties of the BN treated fiber/silicon oxycarbide composite increased by approximately 85% over the asreceived fiber/silicon oxycarbide composite. In addition, the BN-treated fiber/silicon oxycarbide composites showed enhanced strain-to-failure. The high mechanical strengths combined with a damage tolerant failure behavior suggest fiber-matrix bond strength strong enough to impart strength to the ceramic, but weak enough to provide energy absorption and crack deflection.

# References

- N. Chandra, C.R. Ananth, and H. Garmestani, "Micromechanical Modeling of Process-Induced Residual Stresses in Ti-24Al-11Nb/SCS-6 Composite," Journal of Composites Technology & Research, JCTRER, Vol. 16, No.1, January 1994, pp.37-46.
- 2. Lowden, R.A., "Characterization of Fiber/Matrix Interactions in Ceramic Composites"; Dissertation Abstracts International.
- 3. F. Woolley, "Melting/Fining", Engineered Materials Handbook, Vol. 4, ASM, 1991 pp. 386-392.
- 4. G. Ziegler, W. Huttner, "Engineering Properties of Carbon-Carbon and Ceramic-Matrix Composites", Engineered Materials Handbook, Vol. 4, ASM, 1991 p. 841
- 5. A.E. McHale, "Engineering Properties of Glass-Ceramics", Engineered Materials Handbook, Vol. 4, ASM, 1991 p. 875
- 6. A.E. McHale, "Engineering Properties of Glass-Ceramics", Engineered Materials Handbook, Vol. 4, ASM, 1991 pp. 870-871
- 7. A.E. McHale, "Engineering Properties of Glass-Ceramics", Engineered Materials Handbook, Vol. 4, ASM, 1991 pp. 874-875
- 8. A.I. Kingon, R.F. Davis, M.M. Thackeray, "Engineering Properties of Multicomponent and Multiphase Oxides", Engineered Materials Handbook, Vol. 4, ASM, 1991 p. 763
- 9. Kingery, W.D., Bowen, H.K., Uhlmann, "Introduction to Ceramics, Second Edition", John Wiley & Sons, 1976 p.305
- 10. M. Miyayama, K. Koumoto, H. Yanagida, "Engineering Properties of Single Oxides", Engineered Materials Handbook, Vol. 4, ASM, 1991 p. 752.
- 11. J. D. Sibold, "Wear Applications", Engineered Materials Handbook, Vol. 4, ASM, 1991 p. 973.
- 12. P.T.B. Shaffer, "Engineering Properties of Carbides", Engineered Materials Handbook, Vol. 4, ASM, 1991 pp. 806-807.
- 13. Kingery, W.D., Bowen, H.K., Uhlmann, "Introduction to Ceramics, Second Edition", John Wiley & Sons, 1976 pp.79-81
- 14. S. Hampshire, "Engineering Properties of Nitride", Engineered Materials Handbook, Vol. 4, ASM, 1991 pp. 812-813.
- 15. F. V. Tooley, "Fiberglass", Engineered Materials Handbook, Vol. 4, ASM, 1991 pp.

402-407.

- 16. P.F. Aubourg, C. Crall, J. Hadley, R.D. Kaverman, D.M. Miller, "Glass Fibers", Engineered Materials Handbook, Vol. 4, ASM, 1991 pp. 1027-1031.
- 17. D.D. Johnson, H.G. Sowman, "Ceramic Fibers" Engineered Materials Handbook, Vol. 1, ASM, 1991 p. 60.
- 18. N.W. Hansen, "Carbon Fibers", Engineered Materials Handbook, Vol. 1, ASM, 1991 p. 111-113.
- 19. T.Schoenberg, "Boron and Silicon Carbide Fibers", Engineered Materials Handbook, Vol. 1, ASM, 1991 p. 592-593.
- 20. P.T.B. Shaffer, "Engineering Properties of Carbides", Engineered Materials Handbook, Vol. 4, ASM, 1991 pp. 804-805.
- 21. H.T. Larker, "Hot Isostatic Pressing", Engineered Materials Handbook, Vol. 4, ASM, 1991 pp. 195-198.
- 22. D.P. Stinton, T.M. Besmann, R.A. Lowden, B.W. Sheldon, "Vapor Deposition", Engineered Materials Handbook, Vol. 4, ASM, 1991 pp. 215-220.
- 23. L.C.Klein, "Sol-Gel Process", Engineered Materials Handbook, Vol. 4, ASM, 1991 pp. 209-213.
- 24. A.W. Urquhart, "Directed Metal Oxidation", Engineered Materials Handbook, Vol. 4, ASM, 1991 pp. 232-235.
- 25. D.R.Petrak, "Polymer-Derived Ceramics", Engineered Materials Handbook, Vol. 4, ASM, 1991 pp. 223-226.
- 26. Tobin, Leung, Gonzcy "LC3 Summary", Allied Signal, Northrup-Grummon, 1998.
- 27. Tauseef Chaudry, M.S. Thesis 1995, Interphase Diagram
- 28. D.B. Marshall, "An Indentation Method for Measuring Matrix-Fiber Frictional Stresses in Ceramic Composites," J. Am. Ceram. Soc. 67 [12] C-259-60 (1984).
- 29. D.B. Marshall and A.G. Evans, "Failure Mechanisms in Ceramic Fiber/Ceramic Matrix Composites," J. Am. Ceram. Soc. 68 [5] 225-31 (1985).
- 30. K.T. Faber and Daniel R. Mumm, Department of Materials Science and Engineering, Robert R. McCormick School of Engineering and Applied Science, Northwestern University, Evanston, IL 60208.; "Interface Design in Brittle-Brittle Systems," 1994.

- 31. W. Toreki, Polym. News, **16**, 6 (1991)
- 32. Rajendra U. Valdya, Joseph Fernando, K.K. Chawla and M.K. Ferber, "Effect of Fiber Coating on the Mechanical Properties of a Nextel-480<sup>™</sup>-Fiber-Reinforced Glass Matrix Composite." Materials Science and Engineering A150 (2) February 29, 1992, P.P. 161-169.
- 33. Singh, R.N.; Brun, M.K.; "Effect of Boron Nitride Coating on Fiber-Matrix Interactions," Advanced Ceramics Materials 3, (3), May 1988, 235-237.
- 34. Wells, H.K., Beaumont, P.W.R.: J. Mater. Sci. 17, 397 (1982)
- 35. Harris, B. Beaumont, P.W.R., deFerran, E.: J. Mater. Sci. 6, 238 (1971)
- 36. Harris, B., Morley, J., Phillips, D.C.: J. Mater. Sci. 10, 2050 (1975)
- 37. Outwater, J.C., Murphy, M.C.: Proc. 24th Ann. Tech. Conf. SPI, Paper 11-C (1969)
- 38. Mullin, J.V.: Analysis of Test Methods for High Modulus Fibers and Composites, 349, ASTM STP 521, Philadelphia, Pa (1973)
- 39. T.M. Besmann, B.W, Sheldon, R.A. Lowden, and D.P. Stinton, Science, 253, 1104 (1991)
- 40. S. Campbell, and S.T. Gonczy, Cer. Eng. Sci. Pro., **15**/4, 327 (1994)
- 41. R.Y. Leung and M. Glazier, Cer. Eng. Sci. Pro., 15/7-8, 209 (1995)
- 42. W. Zhao, P.K. Liaw, R. Belardinelli, D.C. Joy, C.R. Brooks, and C.J. McHargue, Met. Mat. Trans. A, 31A, 911 (2000)
- 43. P.K. Khandelwal, and W.D. Wildman, Am. Cer. Soc. Bull., 65/2, 326 (1986)
- 44. Allied Signal, Blackglas™ Technology and Applications, An Advanced Ceramic Matrix Material for High Temperature Composites 1994-Product Bulletin.
- 45. Holtz, Allan R., and Grether, Michael F.; "High Temperature Properties of Three Nextel™ Ceramic Fibers." 32nd International Sampe Symposium and Exhibition at Anaheim Convention Center, April 6-9, 1987.
- 46. Pipes, Byron R.; Johnson, D.D. and Kurst, K.; "Nextel 312™ Ceramic Fiber Polymeric Composites." 3-M Technical Bulletin.
- 47. Simpson, F.H. and Veremnieks, J., "Barrier Coated Ceramic Fiber and Coating

- Method"; U.S. Patent #4,605,588, August 12, 1986.
- 48. Rice, R.W.; "BN Coating of Ceramic Fibers for Ceramic Fiber Composites"; U.S. Patent #4,642,271, February 10, 1987.
- 49. Simpson, F.H. and Verzemnieks, J.; "Boron Nitride Coated Ceramic Fiber and Coating Method"; U.S. Patent #4,948,662, August 12, 1986.
- 50. Partlow, Deborah, P.; "A Ceramic-Ceramic Composite with Low Dielectric Constant and Nonbrittle Failure"; Advanced Ceramic Materials, 3, (6), 553-56, 1988.
- 51. Campbell, S. and Gonczy, S.; "In-situ Formation of Boron Nitride Interface Coatings on Nextel 312<sup>™</sup> Continuous Fiber I: Nitriding Process and Blackglas<sup>™</sup> Ceramic Matrix Composite Properties".
- 52. Campbell, S. and Gonczy, S.; "In-situ Formation of Boron Nitride Interfaces on Nextel 312™ Continuous Ceramic Fiber II: Oxidation of Blackglas™ Ceramic Matrix Composites".
- 53. Fernando, J.A.; Chawla, K.K.; Ferber, M.K.; Coffey, D.; "Effect of Boron Nitride Coating on Tensile Strength of Nextel 480™ Fiber"; Materials Science and Engineering, A154, (1992), 103-108.
- 54. Singh, R.N.; Brun, M.K.; "Effect of Boron Nitride Coating on Fiber-Matrix Interactions"; CeramicEng. Sci. Proc. 8, (7-8) P.P. 636-643 (1987).
- 55. Lane, Jay, E.; Pebler, Alfred, R.; "Failure Characteristics of Low Dielectric Constant Ceramic Composites Reinforced with BN-Coated Fibers"; Ceramic Eng. Sci. Proc. 10, (9-10) P.P. 1213-1222, (1989).
- 56. Hazlebeck, D.A.; Glatter, I.K.; Streckert, H.H.; "Novel Sol-Gel Coating Techniques for Ceramic Tows: In-situ Curing vs. Reaction Bonding." Ceramics Eng. Sci. Proc. 12, (7-8), P.P. 1075-1085 (1991).
- 57. S.S. Campbell and S.T. Gonczy, Allied Signal Inc. P.O. Box 5016, Des Plaines, IL 60017-5016, and Edgar Leone, Allied Signal, 101 Columbia Rd, Morristown, NJ 07962, and M.J. McNallan, 2095 ERF, University of Illinois at Chicago, 842 W. Taylor St., Chicago, IL 60607, "The Effect of Processing Parameters on the Surface Nitridation of Nextel 312™ Ceramic."
- 58. Hercules, David M., Hercules, Shirley H., University of Pittsburgh, PA 15260, "Analytical Chemistry of Surfaces, Part I: General Aspects"
- 59. Hercules, David M., Hercules, Shirley H., University of Pittsburgh, Pittsburgh, PA 15260, "Analytical Chemistry of Surfaces, Part II: Electron Spectroscopy"

- 60. Drzal, L.T. and Herrera-Franco, Pedro, J.; "Composite Fiber-Matrix Bond Tests", Engineered Materials Handbook, Vol. 1, ASM, 1991, pp. 391-403
- 61. A.G. Tobin, R.M. Leek, and Tom Donnellan, Northrop Grumman Research & Developement Center, Bethpage, NY 11714, "Process-Performance Relationships in 3-D Blackglas™ Ceramic Composites," Presented at the American Ceramic Society Meeting January 7-12, 1995, Cocoa Beach FL.
- 62. E.J.H. Chen and J.C. Young, Comp. Sci. and Technol., 42, 189 (1991)
- 63. D.H. Grande, J.F. Mandell, and K.C.C. Hong, J. Mat. Sci., 23, 311 (1998)
- 64. Hull, Derek, Cambridge University Press, 1987, "An Introduction to Composite Materials", pp.38-40.
- 65. J. Annamalai, W.N. Gill, and A. Tobin, Cer. Eng. Sci. Pro., July-August, 225 (1995)
- 66. M. Allahverdi, W.R. Cannon, and S.C. Danforth, J. Am. Ceramic Soc., **83**/12, 2929 (2000)
- 67. S. Rangarajan, R. Belardinelli, and P. Aswath, J. Mat. Sci., 34, 515 (1999)
- 68. S.H. Yu, R.E. Riman, S.C. Danforth and R.Y. Leung, J. Amer. Cer. Soc., 78/7, 1818 (1995)
- 69. T. Koufopoulos and P.S. Theocaris, J. Comp. Mat., 3, 308 (1969)
- 70. J.O. Outwater and M.C. Murphy, in Proceeding of the 24th Annual Technical Conference, The Society of the Plastics Industry (1969)
- 71 E.J.H. Chen and R.B. Croman, Comp. Sci. and Technol., **48**(1-4), 173 (1993)
- 72. W. Zhao, P.K. Liaw, R. Belardinelli, D.C. Joy, C.R. Brooks, and C.J. McHargue, Met. and Mat. Trans. A, 31A, 911 (2000)
- 73. F.I. Hurwitz, P. Heimann, S.C. Farmer, and D.M. Hembree, J. Mat. Sci., 28, 6622 (1993)cv

